Precambrian Research 300 (2017) 107–120

Contents lists available at ScienceDirect

Precambrian Research

journal homepage: www.elsevier.com/locate/precamres

Apatite and titanite from the Karrat Group, Greenland; implications for charting the thermal evolution of crust from the U-Pb geochronology of common Pb bearing phases

C.L. Kirkland[a,b,*], J. Hollis[c], M. Danišík[d], J. Petersen[c], N.J. Evans[d], B.J. McDonald[d]

[a] Centre for Exploration Targeting – Curtin Node, The Institute for Geoscience Research, Department of Applied Geology, Western Australian School of Mines, Curtin University, Perth, Western Australia 6102, Australia
[b] Australian Research Council Centre of Excellence for Core to Crust Fluid Systems, Australia
[c] Geology Department, Ministry of Mineral Resources, Government of Greenland, P.O. Box 930, 3900 Nuuk, Greenland
[d] John de Laeter Centre, The Institute for Geoscience Research, Department of Applied Geology and Applied Physics, Curtin University, Perth, Western Australia 6102, Australia

ARTICLE INFO

Keywords:
Titanite
Apatite
U-Pb
Geochronology
Common Pb
Non-radiogenic Pb
Thermochronology

ABSTRACT

Titanite and apatite have Pb closure temperatures of ~700 °C and 450–550 °C, respectively, allowing different points on a cooling trajectory to be determined. However, both phases typically accommodate moderate to significant quantities of common Pb. Understanding the thermal diffusivity of a specific isotopic system in different minerals along with their apparent U-Pb age allows modelling of regional cooling trends. Such cooling trends may provide key evidence for correct interpretation of the measured geochronometer. Specifically, thermal history reconstruction may address questions related to the interpretation of an isotopic date as the time of crystallization versus cooling, or alternatively, as a resetting age. In this work, a case study from metavolcanic rocks of the Karrat Group, West Greenland, is used to inform the U-Pb geochronology of common Pb bearing phases, thermal modelling, and also the regional geology. Magmatic apatite yields a reset U-Pb age of 1826 ± 9 Ma, whereas titanite yields a mean U-Pb age of 1768 ± 8 Ma. The apatite age is interpreted as the time of total resetting during a > 485 °C event. In contrast, the titanite age is interpreted as the time of metamorphic crystallization, consistent with its REE chemistry. Thermal modelling indicates this metamorphic event did not exceed 452 °C. The resetting of the U-Pb system in magmatic apatite is interpreted as a response to the collision between the Rae Craton and the Superior Craton during the Trans-Hudson Orogeny. However, subsequent metamorphic titanite growth is interpreted as distal evidence of an event shared with the Nagssugtoqidian Orogen. The modelled thermal history implies over 100 million years of communal tectonic history between the Nagssugtoqidian and Rinkian Orogens. Of great significance is the fact that both apatite and titanite show distinctly different common Pb compositions. Apatite retains common Pb with a composition similar to ancient common Pb, whereas titanite retains common Pb with a lower $^{207}Pb/^{206}Pb$ ratio implying it was influenced also by Pb from recrystallized precursor U bearing minerals. The common Pb signature in minerals may assist in interpretation of the growth mechanism of the dated phase.

1. Introduction

Titanite (CaTiSiO) and apatite $Ca_5(PO_4)_3(F,Cl,OH)$ can be powerful U-Pb geochronometers (Catanzaro and Hanson, 1971; Hanson et al., 1971; Oosthuyzen and Burger, 1973; Tilton and Grunenfelder, 1968; Chew et al., 2011; Kohn and Corrie, 2011; Spencer et al., 2013; Chew et al., 2014; Kirkland et al., 2016), and have been widely used to delimit post-orogenic cooling and exhumation (Corfu, 1988; Mezger et al., 1989; Tucker et al., 1986; Kirkland et al., 2016; Schwartz et al., 2016). However, both phases often incorporate some amount of common Pb (non-radiogenic Pb) which must be accurately accounted for in order to derive meaningful U-Pb ages.

Apatite is a minor but ubiquitous mineral in most igneous rocks, including those of basaltic composition, and also occurs in metamorphic rocks with pelitic, carbonate, or mafic composition. Apatite can accommodate magmatic water, halogens, S, C, and trace elements

* Corresponding author at: Centre for Exploration Targeting – Curtin Node, The Institute for Geoscience Research, Department of Applied Geology, Western Australian School of Mines, Curtin University, Perth, Western Australia 6102, Australia.
E-mail address: c.kirkland@curtin.edu.au (C.L. Kirkland).

http://dx.doi.org/10.1016/j.precamres.2017.07.033
Received 23 May 2017; Received in revised form 18 July 2017; Accepted 22 July 2017
Available online 08 August 2017

including Sr, U, Th, along with frequently significant quantities of non-radiogenic Pb in its structure (Webster and Piccoli, 2015). Diffusion kinetics of Pb in apatite have been obtained experimentally, yielding nominal closure temperatures of 450–550 °C (Cherniak and Watson, 2000, 2001; Cherniak et al., 1991). Apatite is stable at epidote–amphibolite-facies conditions and, to a significant degree, inert to recrystallization during overprinting metamorphism, even at temperatures higher than the apatite closure temperature for Pb diffusion. Therefore, the U-Pb system in apatite tends to be chiefly controlled through diffusion processes rather than growth or recrystallization (Willigers et al., 2002).

In contrast to apatite, titanite is a widespread accessory mineral with a higher Pb closure temperature of around 700 °C (Cherniak, 1993), near the upper limits of amphibolite facies. The abundance of major and accessory minerals rich in both Ti and Ca leads titanite to frequently form or re-precipitate during metamorphic processes in rocks with suitable bulk chemistry, such as metabasites, calc-silicates, granites to diorites and their metamorphosed equivalents (Scott and St-Onge, 1995). The reactive nature, wide stability range, and high closure temperature of titanite makes it a useful tool for dating metamorphism.

1.1. Common Pb

Of particular importance for titanite and apatite geochronology is an understanding of the quantity and composition of common Pb (e.g. Storey et al., 2006). Common Pb is the non-radiogenic portion of Pb that must be subtracted from the total Pb content in a mineral in order to determine the radiogenic fraction that has time significance. The isotopic composition of common Pb is often assumed based on a terrestrial Pb evolution model (e.g., Cumming and Richards, 1975; Stacey and Kramers, 1975) given an estimated crystallization age for the mineral. For phases such as titanite and apatite, where higher levels of common Pb may be present, the impact of the assumed common Pb composition (e.g. recent or ancient) will be more significant than in a low common Pb phase such as zircon. Common Pb may also be estimated by analysing a coexisting low-U phase, rich in the common Pb component (such as feldspar) to pin the common Pb in the mineral of interest (Catanzaro and Hanson, 1971; Housh and Bowring, 1991). However, it is critical to demonstrate a cogenetic relationship between the phase with radiogenic Pb being dated and the common Pb phase used for the correction. Furthermore, apatite and titanite common Pb can be derived from an evolving source, dissimilar to the source of common Pb in feldspar (Schoene and Bowring, 2006). In addition, further complexity in the form of a variable common Pb composition within a titanite population from a single lithology has also been reported (Essex and Gromet, 2000).

A range of alternative means of correcting for common Pb has been summarised elsewhere (e.g. Storey et al., 2006; Chew et al., 2011) and only a brief review is provided here. The stable non-radiogenic isotope of lead (^{204}Pb) can be utilized as a monitor of the common lead content and is a powerful approach in which the amount of measured ^{204}Pb is related through a Pb isotopic model (e.g. Stacey and Kramers, 1975) to the amount of non-radiogenic Pb present in the signals of ^{206}Pb, ^{207}Pb and ^{208}Pb. The measured Pb ratios can thus be corrected for common lead. However, measuring ^{204}Pb can be challenging to universally apply due to the pervasive presence of Hg in mass spectrometer flow through gas (Ar), which leads to a direct interference of ^{204}Hg on ^{204}Pb (Andersen, 2002). The ^{207}Pb/^{206}Pb composition of the common Pb component is not defined through ^{204}Pb correction. In ^{207}Pb correction, a data point is regressed through a fixed upper ^{207}Pb/^{206}Pb intercept on a Tera and Wasserburg (1972) concordia plot, with the lower intercept from the regression being the ^{207}Pb-corrected ^{238}U/^{206}Pb age of that analysis (Gibson and Ireland, 1996). This method assumes both concordance and a common Pb composition. This approach has been applied to determine the age of Proterozoic and younger titanites where the regression lies at a high angle to the concordia curve (e.g. Kohn and Corrie, 2011; Spencer et al., 2013; Chew et al., 2014). Correction using ^{208}Pb is applicable to low Th/U (e.g., < 0.5) minerals (Williams, 1998; Compston et al., 1992) where no ^{208}Pb is derived from radioactive decay of ^{232}Th so ^{208}Pb can serve as a monitor of the common component. Analogous to the ^{204}Pb correction, the amount of common Pb can be derived through the measured ^{208}Pb and a model defining ^{206}Pb/^{208}Pb or ^{207}Pb/^{208}Pb.

Two additional alternative approaches are particularly relevant to address the common Pb composition of the samples considered in this work. A regression through multiple uncorrected data points plotted on a Tera and Wasserburg (1972) concordia diagram for a cogenetic suite of samples with variable contamination by a single common Pb composition will display a trend to elevated ^{207}Pb/^{206}Pb, reflecting greater common Pb, where the ordinate intercept indicates the ^{207}Pb/^{206}Pb ratio for common Pb. Such unforced regression lines do not assume a specific common Pb composition nor a time of Pb loss. Another powerful approach is the total-Pb/U isochron – a three-dimensional ^{238}U/^{206}Pb vs. ^{207}Pb/^{206}Pb vs. ^{204}Pb/^{206}Pb plot (Ludwig, 1998), which simultaneously determines the initial ^{206}Pb/^{204}Pb and ^{207}Pb/^{204}Pb compositions and age for cogenetic samples. A suite of cogenetic minerals where the spread in ratios is due only to the presence of common Pb will define a line in this space that yields both the smallest age uncertainty of any possible U/Pb or Pb/Pb isochron and information on the ^{204}Pb/^{206}Pb common Pb composition.

In addition to the need to carefully choose a common Pb composition, an important question is whether all common Pb was incorporated into the crystal coeval with its growth or whether it was a more recent addition to the crystal (or indeed the analytical volume – in the case of surface derived common Pb).

Furthermore, mixtures between ancient and recent common Pb are feasible with the proportion of ancient to recent common Pb within a mineral being highly phase-specific. For time resolved analyses, a decreasing ^{204}Pb/^{206}Pb ratio during analysis could imply a surficial common Pb component, whereas consistent ratios could imply a common Pb component bound within the mineral phase itself.

1.2. Closure temperature

A further important concept in the consideration of apatite and titanite geochronology, which arguably is less relevant for minerals that retain radiogenic-Pb at high temperatures (e.g. zircon, monazite, and allanite), is closure temperature (Dodson, 1973). The range of Pb diffusivity in accessory minerals provides the opportunity to reconstruct comprehensive thermal histories using the U-Pb isotopic system. Closure temperature is a function of diffusivity, cooling rate, and effective radius of diffusion domain (Dodson, 1973), and can be constrained by experimental and empirical studies. If all radiogenic daughter isotopes produced in a mineral after crystallization are retained, then an igneous or metamorphic age may be obtained. In contrast, minerals that experienced some degree of daughter loss will yield an underestimated igneous or metamorphic crystallization age. Nevertheless, such ages may still have geological significance in that they can elucidate the thermal history that followed crystallization or the peak temperature. Such ‘thermochronology’ ages can either record the time when the mineral phase cooled to a temperature when it started to accumulate radiogenic daughter product (e.g. cooling age), or result from a partial resetting of the parent-daughter system by a subsequent thermal event, and not necessarily record any specific geological event (e.g. apparent age or mixed age). Daughter isotope loss is generally considered as predominantly diffusive and conceptualised by considering an idealized, spherical mineral grain of specific radius (Dodson, 1986). Under this widely applied model (Dodson, 1986) post-crystallization loss of daughter isotopes occurs exclusively through volume diffusion; the material contiguous to the mineral serves as an infinite sink for daughter isotopes lost from the grain, temperature changes linearly, and the grain acts homogeneously. Using this empirical approach,

closure temperatures have been derived for both titanite and apatite.

Pb diffusion and closure temperatures in apatite crystals have been comprehensively studied (e.g., Cherniak et al., 1991; Krogstad and Walker, 1994; Chamberlain and Bowring, 2001). Comparison of empirical approximations based on interpolation through U-Pb monazite, Rb-Sr mica, and K-Ar mica data with theoretical calculations based on parameters of Cherniak et al. (1991), indicate a Pb closure temperature of c. 620 °C for 100–200 mm apatite grains (Krogstad and Walker, 1994). Other comparative studies of U-Pb, Rb-Sr, and K-Ar behaviour have been used to estimate a closure temperature (of c. 400–500 °C) for Pb diffusion in typical apatite which is lower than the U-Pb system in zircon, monazite, and titanite, but similar to K-Ar in amphibole, and higher than Rb-Sr in biotite (Chamberlain and Bowring, 2001).

Closure temperature estimates for Pb in titanite, based on both empirical and natural data (Gromet, 1991; Mezger et al., 1993; Scott and St-Onge, 1995; Corfu, 1996; Pidgeon et al., 1996; Cherniak, 1993), are in broad agreement that cooling rates of 10–100 °C/Myr from temperatures of 700–800 °C are adequate to cause Pb loss in 2–10 mm titanite grains (Spencer et al., 2013). Total radiogenic Pb loss is empirically predicted in 1 mm radius grains at temperatures ≥750 °C. In contrast Spencer et al. (2013) used a natural dataset to show that titanite was retentive to Pb for tens of millions of years, on length scales of 1 mm, at temperatures as high as 750 °C.

In this work we present results of apatite and titanite U-Pb geochronology from mafic metavolcanic rocks of the Kangigdleq Member, Karrat Group, Greenland. The results place important constraints on the regional thermal history and also have widespread importance for U-Pb geochronology by demonstrating dissimilar common Pb content in magmatic versus metamorphic minerals.

2. Geological setting

The study area lies within the Karrat Group in the southernmost Rae Craton within the 1880 Ma Rinkian Fold Belt, just north of the Aasiaat Domain and the much larger North Atlantic Craton to the south (Fig. 1; van Gool et al., 2002; Connelly and Thrane, 2005; Connelly et al., 2006; St-Onge et al., 2009). The Rae Craton is thought to have amalgamated, first with the Aasiaat Domain – a proposed microcontinent – at c. 1880 Ma during the Rinkian Orogeny (St-Onge et al., 2009) and thereafter, at 1860–1840 Ma, with the North Atlantic Craton to the south during the Nagssugtoquidian Orogeny, the effects of which diminish and disappear north of southern Disko Bay (Fig. 1). The suture between the Rae and North Atlantic Cratons is thought to lie in central Disko Bay (Fig. 1; Connelly and Thrane, 2005; Connelly et al., 2006). The Karrat Group has been correlated over c. 1000 km through west Greenland and Arctic Canada with the typically higher metamorphic grade (upper greenschist to granulite facies) Piling Group on Baffin Island and Piling and Penrhyn Groups on Melville Penninsula (Taylor, 1982; Henderson, 1983). On Baffin Island the Piling Group is intruded by the 1900–1880 Ma Qikiqtarjuaq suite, which is thought to be petrogenetically related to the 1900–1870 Ma Prøven Granite (Thrane et al., 2005; Thrane pers. comm., 2017).

The Karrat Group is a several kilometre thick succession of greenschist to amphibolite (and more locally granulite) facies turbiditic metasedimentary rocks with subordinate quartzite, carbonate, and mafic metavolcanic rocks, exposed along c. 400 km of coastline (Henderson and Pulvertaft, 1967, 1987). The Karrat Group (and correlative Piling Group) shows evidence of a change in provenance up section, from dominantly Archean to an increased Paleoproterozoic source, with deposition occurring after c. 2000 Ma (Kalsbeek et al., 1998; Johns, 2002). The Karrat Group unconformably overlies (Garde and Pulvertaft, 1976) dominantly Mesoarchean felsic orthogneiss basement of the Rae Craton (3100–2980 Ma; Thrane et al., 2003; Connelly et al., 2006), though the basal contact of the Karrat Group is almost everywhere strongly tectonised.

The Karrat Group has been subdivided into a lowermost Qeqertarssuaq Formation, unconformably overlain by the Nûkavsak Formation (Fig. 1; Henderson and Pulvertaft, 1967). The Qeqertarssuaq Formation is approximately 500 m thick and comprises dominantly lower to middle amphibolite facies siliciclastic rocks including quartzite, psammite and semipelitic schist ± calc-silicate rocks (Henderson and Pulvertaft, 1967; Grocott and Pulvertaft, 1990).

The Qeqertarssuaq Formation is unconformably overlain by a ≥5 km section of dominantly greenschist to amphibolite facies metaturbiditic rocks of the Nûkavsak Formation, including the lowermost metavolcanic Kangigdleq Member, which is the subject of this study. The Kangigdleq Member comprises mafic metavolcanic and metavolcaniclastic rocks of alkaline basaltic composition that vary in thickness from tens of metres to over 850 m (Rosa et al., 2016), regionally thinning away from their thickest point (Allen and Harris, 1980). The Kangigdleq Member variably preserves primary volcanic textures including tuff beds, pillows, hyaloclastites, vesicular flows, and volcanic breccias (Allen and Harris, 1980; Rosa et al., 2016). The upper contact of the Kangigdleq Member with the Nûkavsak Formation is transitional over tens of metres. Thin metavolcanic units above the main body of the Kangigdleq Member and within lowermost metaturbiditic rocks of the Nûkavsak Formation indicate that intermittent volcanism continued during deposition of the Nûkavsak Formation (Rosa et al., 2016).

The Nûkavsak Formation is a > 5 km thick succession of monotonous, rhythmically layered, turbiditic metagreywacke, pelite and psammite (Henderson and Pulvertaft, 1967, 1987; Rosa et al., 2016). The Nûkavsak Formation commonly contains mafic volcanic clasts, indicative of reworking of the underlying Kangigdleq Member (Rosa et al., 2016). Already deformed turbidites of the Nûkavsak Formation were intruded by the Prøven Igneous Complex at 1900–1869 Ma (Thrane et al., 2005; Thrane pers. comm., 2017), resulting in granulite-facies metamorphism proximal to the intrusion, and providing a minimum constraint on the age of deposition of the Nûkavsak Formation and fabric formation (Thrane et al., 2005). If this interpretation is correct, the Kangigdleq Member must be older than 1900 Ma, although there is no direct intrusive relationship between the Prøven Igneous Complex and the Kangigdleq Member.

Deformation in the Karrat Group has been divided into 4 main stages. D1 produced tight folds and possibly thrusts, which occur only in the Qeqertarssuaq Formation (Rosa et al., 2016). This was followed by NE- to E-directed thrusting and formation of a penetrative S2 schistosity. D3 produced NW- to W-directed thin- and thick-skinned thrust sheets that dominate the outcrop pattern, and intensified the existing schistosity. Finally D4 produced very large upright to overturned dome-shaped anticlines with tight synclines, and minimal development of tectonic fabric (Grocott and Pulvertaft, 1990; Garde et al., 2003; Sidgren et al., 2006).

3. Sample information

All samples analysed were collected from mafic metavolcanic rocks, interpreted as mafic lavas and tuffs, of the Kangigdleq Member of the Nûkavsak Formation (Fig. 1). Tectonic fabric development in all samples is attributed to D2, which produced NE-vergent thrusts and the main regional metamorphic fabric, and which was intensified during D3.

3.1. (71,66378 N, -52,7737 W; Niaqornakassak)

Sample 571716 is a fine-grained grey amphibolite collected from a c. 100 m thick succession of amphibolites tectonically overlying quartzite of the Qeqertarssuaq Formation on the northeast corner of Qeqertarssuaq Island (Fig. 1). Here the lowermost sequence of amphibolites contain rare-earth-element (REE) mineralization, which has been attributed to metasomatic alteration broadly constrained to around 1860 Ma (Mott et al., 2013). The amphibolites are variably

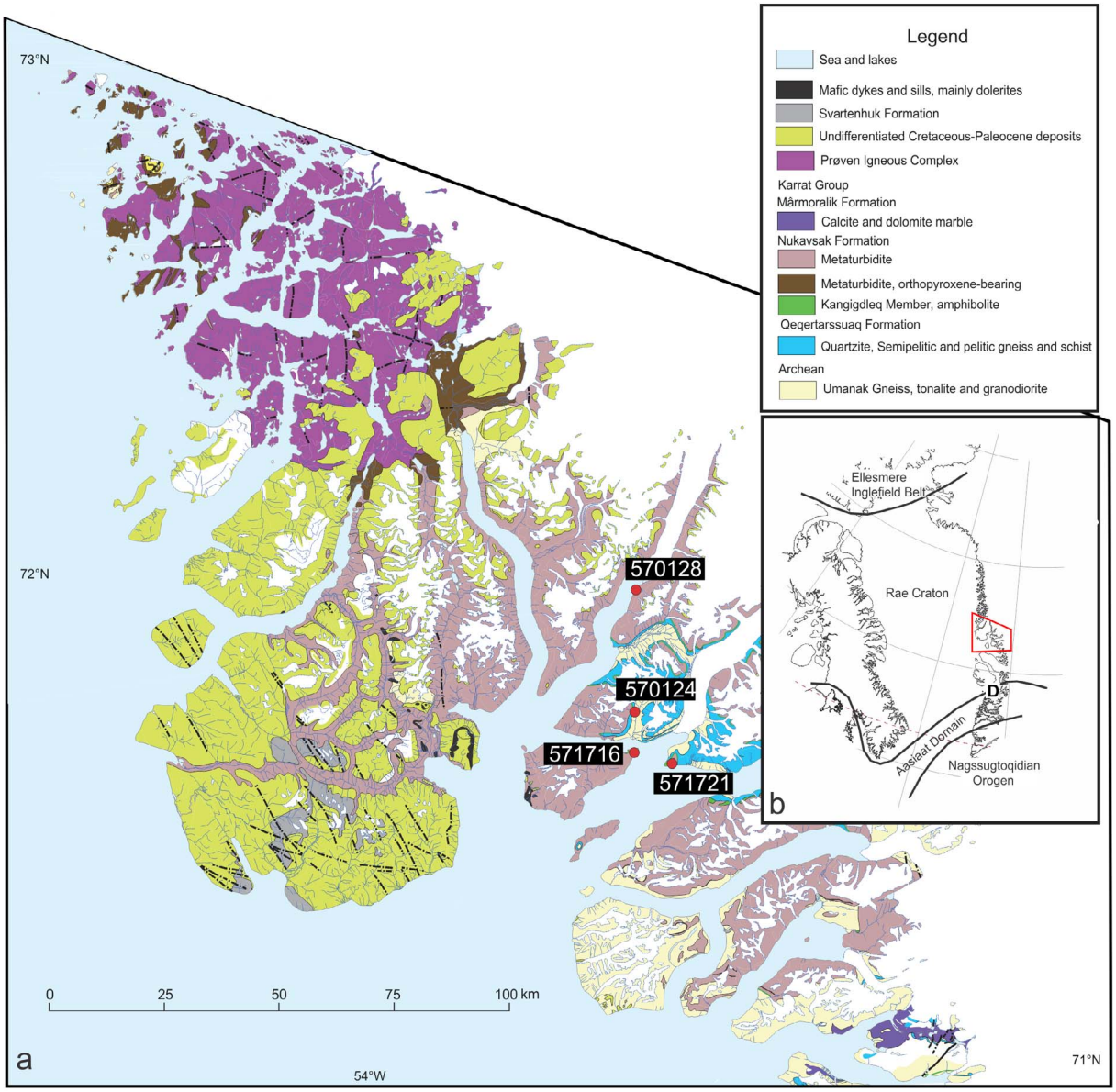

Fig. 1. Geological map of west central Greenland showing the outcrop occurrence of geological units mentioned in the text. Sample locations are shown as circles (modified from Escher, 1985 and Rosa et al., 2016). Inset: Composite geological map highlighting the principal cratonic, supracrustal and tectonic entities, as well as the bounding crustal structures in eastern Canada and West Greenland (modified from St-Onge et al. (2009), Rosa et al., 2016; and Escher, 1980). D denotes Disko Bay.

schistose or massive and have a transitional upper contact with greywacke of the Nûkavsaq Formation. Sample 571716 was collected from a few metres from the REE-mineralised shear zone within the amphibolites. It is a massive fine to medium-grained grey foliated biotite bearing amphibolitic rock with weak schistosity. Hornblende is elongated and prismatic and 1–2 mm long. Plagioclase is 1–3 mm long and elongate and prismatic. Biotite forms flakes 1–2 mm thick and is 0.5 to 1 cm long with aggregates parallel to the foliation. Minor amounts of calcite are found as 1–3 mm euhedral crystals that form irregular aggregates 2–4 mm in diameter.

3.2. (71,97726 N, -52,7472 W; Salliarutsip Kangerlua - Ingia Fjord)

Sample 570128 is a medium-grained amphibolite collected immediately above a tuff layer within the lowermost Nûkavsaq Formation (Fig. 1). The sampled unit consists of a c. 2 m thick package of medium-grained amphibolite with relict primary igneous textures and a weak foliation. The sample contains abundant prismatic black amphibole (1–3 mm) and plagioclase (1–2 mm) that define the foliation. Chlorite occurs along thin fractures. The amphibolite is overlain by a 3–4 m thick coarse-grained sandstone containing thin layers of redeposited volcanic rock fragments.

3.3. (71,63834 N, -52,5704 W; Umiammakku Nuuat)

Sample 571721 was collected from the stratigraphically uppermost section of the Kangigdleq Member. The rock is a dark grey, fine- to medium-grained, strongly planar-foliated amphibolite. The sample contains elongated and prismatic amphibole (1–2 mm), plagioclase (2–3 mm), and biotite (1–2 mm) that define the foliation.

3.4. (71,75000 N, -52,7699 W; Kussinersuup Aaffaa)

Sample 570124 was collected from a > 50 m thick section of amphibolite with a sharp lower contact to quartzite of the Qeqertarssuaq Formation with a transitional upper contact into metagreywackes of the

Nûkavsaq Formation. The sample was collected from the lowermost fine-grained, schistose, dark greenish grey foliated amphibolite. The amphibolite is sheared and no relict texture is preserved. The sample contains amphibole (1–2 cm), plagioclase (1–2 mm), biotite, chlorite, calcite and accessory pyrite. Chlorite is fine grained and constitutes approximately 10% of the rock. Calcite is found in thin veins that are typically less than 1 mm in thickness and 1–2 cm long. Disseminated pyrite is less than 1 mm in diameter and is found as small cubic crystals that constitute less than 1% of the rock.

4. Methods

Titanite and apatite, along with all other heavy phases, were separated by SelFrag (selective fragmentation system), utilizing a high voltage electrodynamic disaggregation. The disaggregated rock was elutriated, dried, magnetically and density separated. Density separation was completed using sodium polytungstate. The resultant heavy fraction was mounted in epoxy resin and polished to half grain thickness. Mounts were then imaged using a TESCAN Integrated Mineral Analyser (TIMA). TIMA outputs included backscatter electron images and also phase maps determined through energy dispersive spectroscopy.

Titanite and apatite targets for LA-ICPMS were selected based on both backscatter and phase identification images. All LA-ICPMS analysis was performed at the GeoHistory Facility in the John de Laeter Centre, Curtin University, Perth, Australia. Individual titanite or apatite grains (mounted and polished in 25 mm epoxy rounds) were ablated using a Resonetics RESOlution M-50A-LR system, incorporating a COMPex 102 193 nm excimer UV laser. For quadrupole LA-ICPMS, a 50 μm diameter laser spot, 5 Hz laser repetition rate, and laser energy of 1.4 J cm^{-2} were utilized. Isotopic intensities were measured using an Agilent 7700 s quadrupole ICPMS, with high purity Ar as the plasma gas (1 L min^{-1}). The experiment used the following schedule: 2 × 1 s cleaning pulse; 10 s delay; 15 s background measurement; 30 s of measurement; 15 s of cell washout. The sample cell was flushed by ultrahigh purity He (350 mL min^{-1}) and N (3.8 mL min^{-1}).

Quadrupole LA-ICPMS apatite mass spectra were reduced using the VizualAge_UcomPbine data reduction scheme in Iolite (Chew et al., 2014; Paton et al., 2010) and in-house excel macros. The primary age standard was Mount McClure (524 Ma; Schoene and Bowring, 2006) with MAD (485 ± 1.7 Ma; Thomson et al., 2012) and FC-Duluth (1099 ± 1 Ma zircon; Schmitz et al., 2003; 1094 ± 35 Ma apatite; Thomson et al., 2012) employed as secondary standards to verify the procedure. Regressions from Stacey and Kramers (1975) contemporaneous common Pb through both secondary standards, treated as unknowns, yielded ages within analytical uncertainty of the accepted values (MAD = 485 ± 7 Ma, MSWD = 0.3; FC-Duluth = 1095 ± 13, MSWD = 1.7). Ages were calculated using a regression approach that provides both the common Pb composition and age of the radiogenic component.

In addition to the quadrupole dataset, a single apatite sample (571716) was analysed using single stream multi-collector (MC) ICPMS (Nu plasma II). The aim was to measure precise ^{204}Pb (and ^{202}Hg) in order to perform a ^{204}Pb correction and verify the ages obtained using the regression approach. The method of common Pb correction described in Thomson et al. (2012) was applied. Following two cleaning pulses and a 40 s period of background analysis, samples were spot ablated for 30 s at a 4 Hz repetition rate using a 75 μm beam and laser fluence at the sample surface of 2 J cm^{-2}. An additional 20 s of baseline was collected after ablation. The sample cell was flushed with ultrahigh purity He (320 mL min^{-1}) and N_2 (1.2 mL min^{-1}) and high purity Ar was employed as the plasma carrier gas (1 L min^{-1}). U and Pb isotopes were counted simultaneously in static mode, using Faraday detectors for ^{238}U and ^{232}Th and ion counters for ^{208}Pb, ^{207}Pb, ^{206}Pb, ^{204}Pb, ^{202}Hg and ^{200}Hg.

Titanite mass spectra were reduced using the U_Pb_geochron4 data reduction scheme in Iolite (Chew et al., 2014; Paton et al., 2010), and in-house excel macros as the primary standard (OLT) contains neglible common Pb. The primary age standard used for titanite analysis was OLT (1015 ± 2 Ma; Kennedy et al., 2010) with BLR (1047 ± 0.4 Ma; Aleinikoff et al., 2007) employed as a secondary standard, to verify the procedure. Regressions from contemporaneous common Pb through uncorrected data for BLR, treated as an unknown, yielded an age of 1046 ± 4 Ma (MSWD = 0.4; n = 33), within analytical uncertainty of the accepted value.

In order to constrain the final cooling of the investigated region through the ~65 °C isotherm, apatite from sample 570124 were analysed by the conventional (U-Th)/He method. Analytical procedures followed the protocols described in Danišík et al. (2012a, 2012b). In brief, six crystals were extracted from the grain mount used for LA-ICPMS analysis and loaded in Pt tubes. ^{4}He was extracted from single-grain aliquots under ultra-high vacuum by heating to ~960 °C using a diode laser, and measured by isotope dilution on a Pfeiffer Prisma QMS-200 mass spectrometer. Following He measurements, the apatite crystals were spiked with ^{235}U and ^{230}Th and dissolved in nitric acid. The solutions were analysed by isotope dilution for U and Th, and by external calibration for Sm on an Agilent 7500 ICP-MS. The total analytical uncertainty was calculated as the square root of the sum of the squares of uncertainty on He and weighted uncertainties on U, Th, Sm, and He measurements.

5. Geochronology results

5.1. Apatite U-Pb

5.1.1. 571716

Apatite crystals from 571716 are equant, euheral to anhedral, and some are traversed by curvilinear fractures filled with calcite or actinolite. The grain size of apatite is dominated by crystals of c. 105 μm length with a maximum of 206 μm. Titanite is not included in apatite, with the only inclusions in apatite being calcite and actinolite. Apatite U content ranges from 0.3 ppm to 19.3 ppm, with a median of 5.4 ppm and Th ranges from 0.1 ppm to 47.2 ppm with a median of 1.3 ppm. 125 U-Pb analyses were performed on apatite crystals. A Tera and Wasserburg plot of apatite analytical results from 571716 defines a discordant array that spreads between a $^{207}Pb/^{206}Pb$ value of 0.98 ± 0.013 at the ordinate intercept to a lower intercept on Concordia of 1803 ± 19 Ma (MSWD = 2.3; Appendix Table 1; Fig. 2). Five apatite grains from this sample with lower amounts of common Pb (as estimated by F207%) were selected for further analysis using the LA-MC-ICPMS setup. All five grains yield between 12 and 24% common Pb as measured by F204%. ^{204}Pb corrected ratios yield a concordia age of 1805 ± 21 Ma (MSWD = 2.0) identical to the age of the lower intercept from the quadrupole dataset (Fig. 2).

5.1.2. 570128

Apatite crystals from 570128 are equant and euheral to anhedral. The grain size of apatite is dominated by crystals of c. 100 μm length with a maximum of 174 μm. 64.0% of apatite separated from 570128 is in discrete grains with no inclusions. Apatite is included within titanite, but titanite is not included in apatite. Apatite is included within pyrite. The only inclusions in apatite are wollastonite, anorthite and actinolite. Apatite U content ranges from 0.1 ppm to 16.1 ppm, with a median of 0.9 ppm and Th ranges from 0.04 ppm to 3.9 ppm with a median of 0.3 ppm. 60 analyses were performed on apatite crystals. A Tera and Wasserburg plot of apatite analytical results from 570128 defines a discordant array that spreads between a $^{207}Pb/^{206}Pb$ value of 0.90 ± 0.024 at the ordinate intercept to a lower intercept on Concordia of 1725 ± 55 Ma (MSWD = 2.8; Appendix Table 1; Fig. 2).

5.1.3. 571721

Apatite crystals from 571721 are equant and euheral to anhedral.

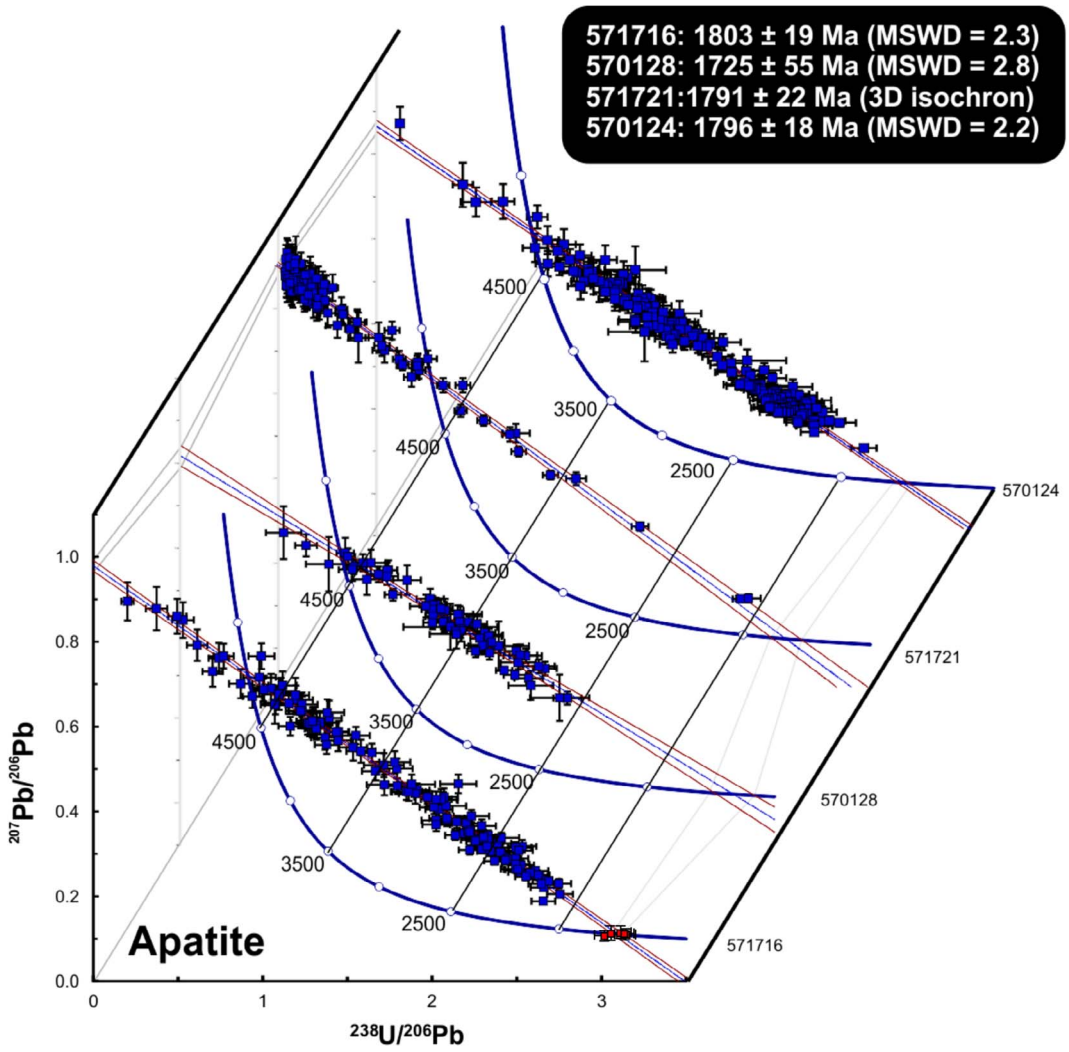

Fig. 2. Stacked Tera and Wasserburg concordia diagram for apatite samples (quadrupole LA-ICPMS are shown as blue squares) with free linear regressions defining a mixture between radiogenic and common Pb components. Two sigma uncertainties on data defined regressions are shown as red lines. Both upper (common $^{207}Pb/^{206}Pb$) and lower (radiogenic $^{207}Pb/^{206}Pb$) intercepts are connected between samples as a visual aid to judge similarity. ^{204}Pb corrected MC-LA-ICPMS data for sample 571716 are shown as red squares. (For interpretation of the references to colour in this figure legend, the reader is referred to the web version of this article.)

The apatite is dominantly c. 70 μm in length but ranges up to a maximum of 194 μm. Only anorthite and calcite are included in apatite. Apatite is included within scheelite. Apatite U content ranges from 0.2 ppm to 136.3 ppm, with a median of 0.7 ppm and Th ranges from below detection limit to 1040 ppm with a median of 0.2 ppm.124 U-Pb analyses were performed on apatite crystals. A Tera and Wasserburg plot of apatite from 571721 defines a discordant array that spreads between a $^{207}Pb/^{206}Pb$ value of 0.996 ± 0.0052 at the ordinate intercept to a lower intercept on Concordia of 1853 ± 48 Ma (MSWD = 2.9) Contemporaneous common Pb at 1853 Ma for the Stacey and Kramers Pb model is $^{207}Pb/^{206}Pb$ = 0.99 (Stacey and Kramers, 1975), similar to the ordinate intercept (Appendix Table 1; Fig. 2). Due to the relatively high ^{204}Pb intensity during analysis of this sample, accurate $^{204}Pb/^{206}Pb$ ratios could be determined for some analyses, which affords the opportunity to utilize a 3 D isochron approach for this sample. A subset of 52 analyses where $^{204}Pb/^{206}Pb$ ratios could be successfully measured yield a 3-D isochron Concordia plane (MSWD = 2.3) with an intercept ellipse of 1787 ± 29 Ma (2σ), with common Pb plane intercepts at $^{206}Pb/^{204}Pb$ = 15.63 ± 0.21 and $^{207}Pb/^{204}Pb$ = 15.95 ± 0.24. The common Pb intercept on the $^{207}Pb/^{204}Pb$ versus $^{206}Pb/^{204}Pb$ plane is imprecisely determined but is close to 1800 Ma Stacey and Kramers model $^{207}Pb/^{206}Pb$, but with higher Mu ($^{238}U/^{204}Pb$), implying a radiogenic upper crustal source of ancient common Pb.

5.1.4. 570124

Apatite crystals from 570124 are equant and euheral to anhedral. Apatite grains are predominantly c. 70 μm in length but range up to a maximum of 264 μm (Fig. 3). Apatite contains inclusions of anorthite, actinolite, and wollastonite, but is not included in other phases. Apatite U content ranges from 0.5 ppm to 28.6 ppm, with a median of 7.0 ppm and Th content ranges from below detection to 20.8 ppm with a median of 0.4 ppm. 184 U-Pb analyses were performed on apatite crystals. A Tera and Wasserburg plot of apatite analytical results from 570124 defines a discordant array that spreads between a $^{207}Pb/^{206}Pb$ value of 0.963 ± 0.014 at the ordinate intercept to a lower intercept on Concordia of 1796 ± 18 Ma (MSWD = 2.2; Appendix Table 1; Fig. 2).

5.1.5. Apatite U-Pb summary

All apatite samples define arrays on Tera and Wasserburg plots in which individual analyses scatter along lines reflecting the contribution of both radiogenic and common Pb. The samples yield similar lower intercepts and a regression through all data yields a lower intercept of 1826 ± 9 Ma (MSWD = 2.8), interpreted to reflect the best estimate of the time of resetting during a post magmatic thermal overprint. This lower intercept is consistent with an age calculated using ^{204}Pb

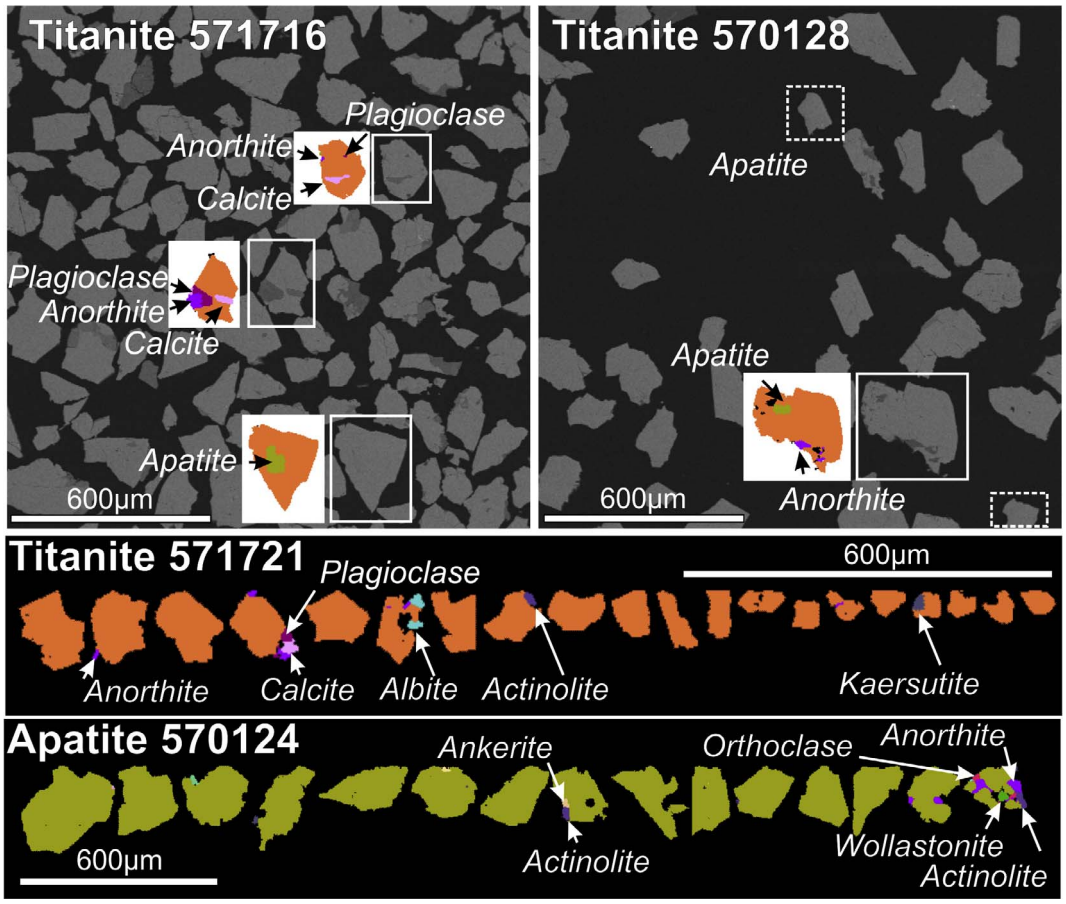

Fig. 3. Composite image of titanite and apatite grains. Samples 571716 and 570128 backscatter image with insets of TIMA phase identification grain maps (entire apatite grains are shown within dashed lines). Sample 571721 TIMA phase identification map of titanite with inclusions indicated. Sample 570124 TIMA phase identification map of apatite with inclusions indicated.

correction. All apatite samples yield comparable upper intercepts with $^{207}Pb/^{206}Pb$ ratios (e.g. 0.986 ± 0.005) similar to 1800–1900 Ma common Pb of the Stacey and Kramers (1975) Pb model (e.g. 0.98–0.99), consistent with ancient common Pb incorporation during crystal growth (Fig. 2).

5.2. Apatite (U-Th)/He

Seven apatite crystals of sample 570124 yielded (U-Th)/He ages from 37.3 ± 2.8 to 58.5 ± 5.9 Ma with a weighted average of 44.5 ± 7.0 Ma (Appendix Table 2). Individual replicates overlap within two sigma uncertainty of the mean and show good reproducibility for this technique. The measured (U-Th)/He ages suggest cooling of the sample through the ~80–40 °C temperature range during Eocene times.

5.3. Titanite U-Pb

5.3.1. 570128

Titanite crystals from 570128 are anhedral and dominantly c. 110 µm in length but range up to a maximum of 273 µm (Fig. 3). Titanite contains inclusions of apatite, anorthite and actinolite. Titanite U content ranges from 0.9 ppm to 114 ppm, with a median of 12 ppm and Th ranges from 0.2 ppm to 26 ppm with a median of 4 ppm. The median Zr content is 191 ppm. 205 U-Pb analyses were performed on titanite crystals. A Tera and Wasserburg plot of titanite results from 570128 is clustered around Concordia and stretching towards common Pb with four analyses yielding highly elevated common Pb. This dataset yields a regression with $^{207}Pb/^{206}Pb$ value of 0.78 ± 0.039 at the ordinate intercept and a lower intercept on Concordia of 1771 ± 13 Ma (MSWD = 5.2), interpreted to reflect a mixture between common and radiogenic Pb components. Model contemporaneous common Pb at 1770 Ma has a $^{207}Pb/^{206}Pb$ ratio of 0.98 (Stacey and Kramers, 1975), considerably greater than the ordinate intercept of 0.78 for the regression (Appendix Table 3; Fig. 4). Four analyses have extreme common Pb content (F207% > 75), although time resolved compositional and isotopic spectra for these ablations do not indicate the presence of intercepted inclusions. These four analyses have low U contents of less than 2 ppm. The regression through all data has scatter in excess of that which can be accounted for by solely analytical uncertainties and implies some degree of radiogenic-Pb loss and / or variable common Pb composition. However, forty three analyses with low amounts of common Pb as estimated by F207% yield a Concordia regression that is insensitive to the common Pb composition, with lower intercepts ranging between 1760 ± 11 Ma (MSWD = 2.1) for Stacey and Kramers (1975) ancient common Pb, 1761 ± 10 Ma (MSWD = 1.9) for Stacey and Kramers (1975) recent common Pb, to 1762 ± 11 Ma (MSWD = 1.9; upper intercept = 0.71 ± 0.15) for a free regression. All lower intercepts are within uncertainty of the regression through all data (1771 ± 13 Ma). The free regression through the most concordant data is interpreted as the most conservative age estimate.

5.3.2. 571716

Titanite from 571716 is anhedral and dominated by crystals of c. 110 µm length, with a maximum grain length of 271 µm (Fig. 3). Titanite contains inclusions of apatite, calcite, anorthite and other more Na rich plagioclaise, and ferro-actinolite. Titanite U content ranges

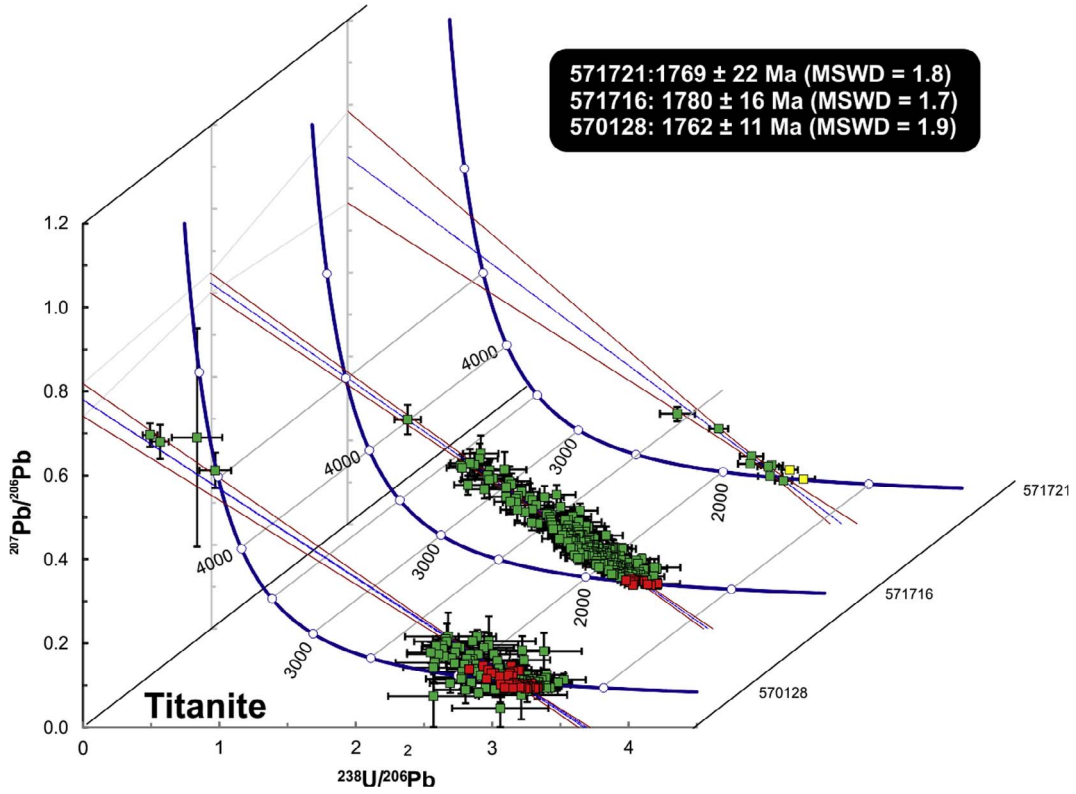

Fig. 4. Stacked Tera and Wasserburg concordia diagram for titanite samples with free linear regressions defining a mixture between radiogenic and common Pb components. Two sigma uncertainties on regressions are shown as red lines. Both upper (common $^{207}Pb/^{206}Pb$) and lower (radiogenic $^{207}Pb/^{206}Pb$) intercepts are connected between samples as a visual aid to judge similarity. (For interpretation of the references to colour in this figure legend, the reader is referred to the web version of this article.)

from 2 ppm to 123 ppm, with a median of 11 ppm and Th content ranges from 0.2 ppm to 61 ppm with a median of 7 ppm. The median Zr content is 153 ppm. 264 U-Pb analyses were performed on titanite crystals. A Tera and Wasserburg plot of titanite results from 571716 defines a discordant array that spreads between a $^{207}Pb/^{206}Pb$ value of 0.823 ± 0.025 at the ordinate intercept to a lower intercept on Concordia of 1771 ± 11 Ma (MSWD = 2.7), interpreted to reflect a mixture between common and radiogenic Pb components (Appendix Table 3; Fig. 4). Contemporaneous common Pb at 1770 Ma has a $^{207}Pb/^{206}Pb$ ratio of 0.98 (Stacey and Kramers, 1975), considerably greater than the ordinate intercept of 0.83. Thirteen analyses with the lowest amount of common Pb as estimated by F207% (e.g. F207% ≤ 1.1) yield a regression that is insensitive to the common Pb composition, with lower intercepts ranging from 1780 ± 16 Ma (MSWD = 1.7) for a free regression, through 1786 ± 17 Ma (MSWD = 1.8) for Stacey and Kramers (1975) recent common Pb, to 1787 ± 17 Ma (MSWD = 1.8) for Stacey and Kramers (1975) ancient common Pb. All lower intercepts are within uncertainty of the regression through all data (1771 ± 11 Ma). The free regression through the most concordant data is interpreted as the most conservative age estimate.

5.3.3. 571721

Only a small number of grains were recovered from this sample. Titanite crystals from 571721 are anhedral and dominantly c. 120 μm in diameter (Fig. 3). Titanite U content ranges from 5 ppm to 77 ppm, with a median of 32 ppm and Th content ranges from 1 ppm to 35 ppm with a median of 16 ppm. The median Zr content in the titanite is 176 ppm. 10 U-Pb analyses were performed on titanite crystals. Two analyses, located on fractures, appear to have recently lost minor amounts of radiogenic-Pb and are excluded from further discussion. A Tera and Wasserburg plot of the remaining data from 507121 defines a discordant array that spreads between a $^{207}Pb/^{206}Pb$ value of 0.87 ± 0.11 at the ordinate intercept to a lower intercept on Concordia of 1769 ± 22 Ma (MSWD = 1.8), interpreted to reflect a mixture between common and radiogenic Pb components (Appendix Table 3; Fig. 4). Contemporaneous common Pb at 1770 Ma has a $^{207}Pb/^{206}Pb$ ratio of 0.98 (Stacey and Kramers, 1975), considerably greater than the ordinate intercept of 0.87.

3.3.4. Titanite U-Pb summary

Best age estimates for all titanite samples are identical within uncertainty and together yield a weighted mean age of 1768 ± 8 Ma (MSWD = 1.7). Upper intercepts from regressions through all data for all samples yield a weighted average $^{207}Pb/^{206}Pb$ ratio of 0.813 ± 0.068 (MSWD = 2.3), distinctly lower than contemporaneous (e.g. $^{207}Pb/^{206}Pb^{@1760\ Ma} = 0.99$) common Pb for any terrestrial Pb evolution model (Fig. 4). Furthermore, this $^{207}Pb/^{206}Pb$ ratio is slightly lower than typical modern day common Pb (e.g. $^{207}Pb/^{206}Pb^{@0\ Ma} = 0.83$), which suggests that the common Pb component in the titanite is a mixture with ancient Pb derived from U bearing phases recrystallized during metamorphism.

6. Discussion

6.1. Petrogenetic implications

Apatite occurs mostly as equant, euhedral to subhedral, homogeneous crystals partially enclosed in the major primary minerals. The grain shapes and textural relationships of apatite are indicative of a primary magmatic origin and its U-Pb age interpreted as the time of resetting during a thermal event at ≥1826 ± 9 Ma. The most typical occurrence of titanite is as anhedral and irregular grains frequently containing inclusions of apatite, whereas apatite has not been observed to contain inclusions of titanite. These observations suggest that apatite growth pre-dates titanite growth, consistent with our age data. All

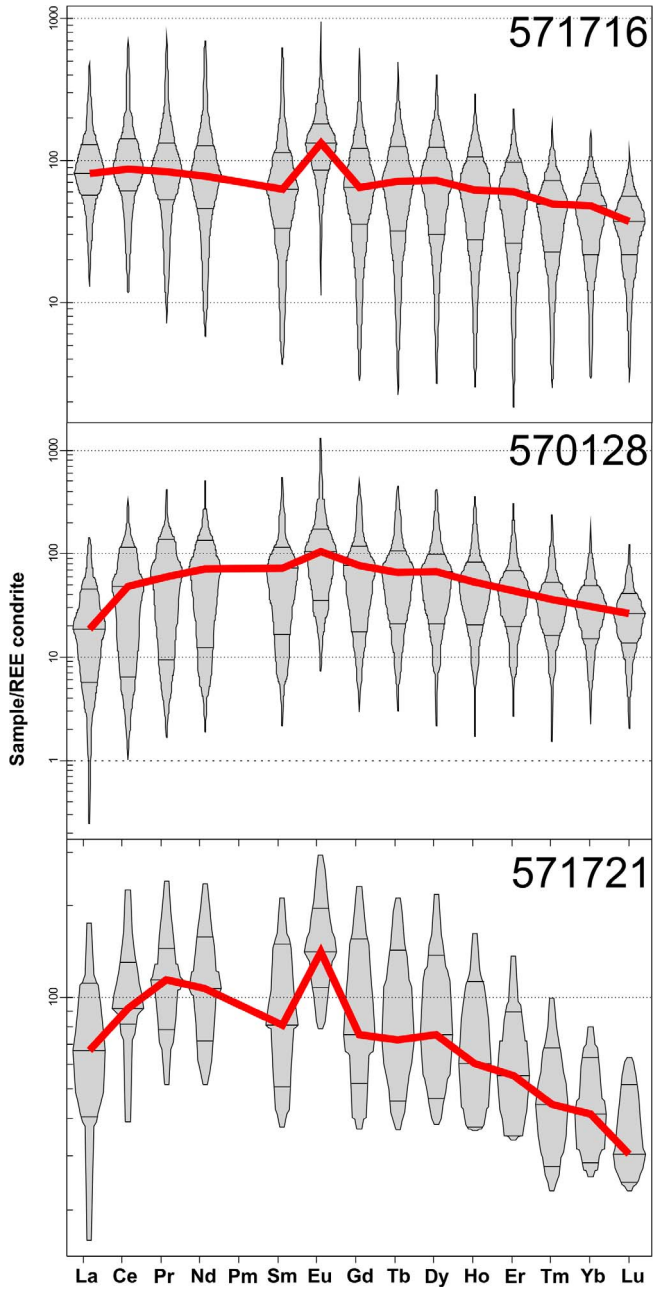

Fig. 5. Chondrite-normalized REE patterns of titanite samples from the Karrat Group, Rae Craton, Greenland. Range of elemental values described by box-percentile plot. Median value indicated by solid red line. (For interpretation of the references to colour in this figure legend, the reader is referred to the web version of this article.)

titanite grains are developed parallel to the S2-3 metamorphic foliation in the rock.

The REE geochemistry of the titanite can be distinctive for different growth environments. Magmatic titanite has been recognised to have higher HFSE (Sn, Y, Nb, Ta, Mo, Zr, Hf, Th, and U) and REE compared to hydrothermal titanite. Magmatic titanite tends to also be enriched in Ti, but depleted in Al, F, and Fe^{3+} compared to hydrothermal titanite (Broska et al., 2007; Morad et al., 2009; Xie et al., 2010). Metamorphic titanite may show similarities to magmatic titanite, depending on the other competing mineral phases developing during metamorphism (Che et al., 2013). The REE pattern for titanite samples 571716, 570128, and 571721 is (on average) characterized by low total REE content (median; 571716 = 258, 570128 = 195, 571721 = 290), positive Eu anomalies, and depletion in both heavy and light REE (Appendix Table 4). Specifically, 571716 and 571721 have weak LREE depletion relative to HREE, whereas 570128 has similar depletion of both LREE and HREE (Fig. 5). The titanite REE patterns in the Karrat samples are similar to metamorphic-hydrothermal titanite (Morad et al., 2009; Xie et al., 2010). Karrat metavolcanic titanite is interpreted to reflect a metamorphic-hydrothermal phase and its U-Pb systematics could conceivably reflect either cooling after a metamorphic-hydrothermal event or alternatively, correspond to the direct timing of that metamorphic-hydrothermal episode if the titanite grew below the Pb diffusion temperature for grains of this size.

6.2. Thermal history reconstruction

The ability to model the behaviour of isotope diffusion and extrapolate it to geological timescales, makes it possible to predict how that system will evolve for a given time-temperature (t–T) history. Hence, using the measured present-day condition of a thermochronometric system (e.g. apatite and titanite U-Pb, apatite U-Th/He) it is feasible to generate a modelled t–T history (Ketcham, 2005; Gallagher, 2012), and to use this to evaluate geological questions related to the thermal history and feasibility of t–T paths. In order to address questions related to the thermal history of the investigated rocks and to understand the timing of tectonometamorphic processes in the region, we attempted to reconstruct a thermal history consistent with all available geochronological data.

The thermal history was modelled using the HeFTy program (Ketcham, 2005), which allows simultaneous reconstruction of time-temperature paths for multiple thermochronometric systems for which diffusion kinetics data are known. The objectives of the modelling were: (i) to reconstruct a thermal trajectory that reconciles the available geochronological data (i.e., apatite U-Pb, titanite U-Pb, hornblende Ar-Ar, muscovite Ar-Ar, and apatite (U-Th)/He ages) to help unravel the meaning of the measured ages (e.g. crystallization, partial resetting or cooling), and (ii) to constrain minimum and maximum temperatures and durations of thermal events. The model was parameterized as follows:

Diffusion kinetic parameters for apatite U-Pb, titanite U-Pb, hornblende Ar-Ar, muscovite Ar-Ar, and apatite (U-Th)/He systems were adopted from Cherniak et al. (1991), Cherniak (1993), Harrison et al. (1991), Hames and Bowring (1994), and Farley (2000), respectively. Radii of the spherical diffusion domains were 33 μm (apatite U-Pb), 37 μm (titanite U-Pb) and 28 μm (apatite (U-Th)/He), based on the measured average size of the analysed crystals. Radii of the spherical diffusion domain for both hornblende and muscovite $^{40}Ar/^{39}Ar$ was assumed to be 100 μm as there are no literature data on the size of analysed grains available, although this has little effect on the resultant model and no influence on the main conclusions. Representative measured ages that were modelled include 1826 ± 9 Ma for apatite U-Pb (this study), 1768 ± 8 Ma for titanite U-Pb (this study), 44.5 ± 7 Ma for apatite (U-Th)/He (this study), 1785 ± 8.8 Ma hornblende $^{40}Ar/^{39}Ar$ (weighted average from Sidgren et al. (2006)) and 1681 ± 14 Ma muscovite (weighted average from Sidgren et al. (2006)).

The starting point of the t–T path was set as T = 10 °C at ~1900 Ma, which is the presumed depositional age of the volcano-sedimentary formation inferred from intrusive constraints (Thrane et al., 2005) and detrital zircon U-Pb data (Kalsbeek et al., 1998; Thrane, pers. comm). After deposition, the sequence was buried and metamorphosed at temperatures that must have reset the U-Pb system in primary apatite. To test the timing and minimum temperatures of this event, we set a constraint at 450–700 °C and 1860–1790 Ma. Following this thermal maximum, the rocks likely cooled as there is no evidence for further heating or thermal stagnation, hence another constraint at 310–400 °C and 1820–1780 Ma was introduced to reflect this process. The titanite U-Pb age of 1768 ± 8 Ma is interpreted to reflect a metamorphic – hydrothermal event consistent with the titanite trace element data and

its growth within the metamorphic foliation. To test the duration and minimum temperatures of this thermal maximum, we set a constraint at 370–800 °C and 1780–1740 Ma. This second thermal maximum was followed by a regional cooling below ~350 °C as recorded by muscovite $^{40}Ar/^{39}Ar$ age of 1681 ± 14 Ma (Sidgren et al., 2006). Accordingly, we set a constraint at 200–350 °C and 1690–1630 Ma. The end of the tT path was set to T = −15 °C at 0 Ma according to the present-day annual mean surface temperature. An inverse modelling approach using a Monte-Carlo search method was then applied to find thermal trajectories that could reconcile the pre-defined parameters and constraints.

After iterative searches we found that the apatite U-Pb age of 1826 ± 9 Ma and titanite U-Pb age of 1768 ± 8 Ma could not be modelled together when conventional diffusion kinetic parameters and grain size were considered. This is unsurprising because the closure temperature of the apatite U-Pb system (c. 450 °C) is lower than the closure temperature of titanite U-Pb (c. 550 °C) and therefore titanite U-Pb ages should be older than apatite U-Pb ages obtained from the same rock if they grew during the same event, which is clearly not the case here. This finding strongly supports the suggestion that titanite formed (crystallized) at a temperature below the closure temperature of the apatite U-Pb system. When titanite is considered as a phase that crystallized below its Pb diffusion temperature, and therefore its U-Pb date reflects a metamorphic crystallization age, we were able to reconstruct thermal trajectories that reproduced all other measured chronometers (Fig. 6).

The major findings of the thermal modelling can be summarized as follows: Minimum temperatures reached during the first thermal maximum at ≥1826 ± 9 Ma must have been > 485 °C in order to fully reset the U-Pb system in apatite. Cooling following apatite resetting has few firm temporal constraints. Nonetheless, a second heating event is recorded by crystallization of metamorphic titanite at 1768 ± 8 Ma. According to the thermal modelling results, maximum temperatures for this second metamorphic event could not have exceeded 452 °C, otherwise the apatite U-Pb system would be (partially) reset again and yield highly scattered U-Pb results, which is not the case. The thermal modelling results also suggest that hornblende Ar-Ar ages of 1785 ± 9 Ma (Sidgren et al., 2006) cannot be related solely to cooling, but must instead represent apparent ages influenced by partial resetting during this second thermal event, consistent with the variability displayed in the Ar-Ar step-heating gas release spectra. An interpretation of partial Ar-Ar resetting is also consistent with other Ar-Ar and K-Ar hornblende age data from further south in the Rinkian Orogen, which yield dispersed ages that scatter between the Archaean and c. 1765 Ma, indicating partial resetting of these isotopic systems (Rasmussen and Holm, 1999). If our interpretation of the mineral geochronometers is correct then the thermal history implied calls into question the inferred regional uplift rates for such partially reset systems (e.g. Sidgren et al., 2006). The second thermal event was followed by moderate cooling to the 300 °C isotherm at c. 1680 Ma as recorded by muscovite Ar-Ar data. From this point, no information on the cooling history is available until the Eocene period as recorded by apatite (U-Th)/He data, when the samples either cooled through near-surface temperatures (80–40 °C) or where briefly heated by a plume traversing below Greenland (Larsen et al., 2016; Fig. 6).

6.3. Geological significance of thermal history

U-Pb apatite and titanite age data presented here demonstrate that, in the period c. 1830–1765 Ma, Rinkian orogenesis was characterised by punctuated thermal events at decreasing temperatures, rather than by slow cooling (cf. Sidgren et al., 2006). The U-Pb system in magmatic apatite was reset at > 485 °C at ≥1826 ± 9 Ma, probably during regional D2 NE- to E-directed thrusting and S2 foliation development. This thermal event may have been responsible for limited development of 1840–1830 Ma metamorphic zircon rims in the Prøven Igneous Complex and Nûkavsak Formation (Thrane, pers comm.), and whole rock–garnet Sm-Nd and Lu-Hf ages of 1820–1800 Ma for the Prøven Igneous Complex (Thrane et al., 2005), previously attributed to regional amphibolite to granulite-facies metamorphism during post-collisional shortening (Thrane et al., 2005). Subsequent metamorphic titanite growth at 1765 ± 7 Ma must have occurred at lower temperatures (< 485 °C), probably during foliation intensification during D3 NW- to W-directed thrusting. The titanite ages cannot reflect isotopic closure during cooling from the same metamorphic event in

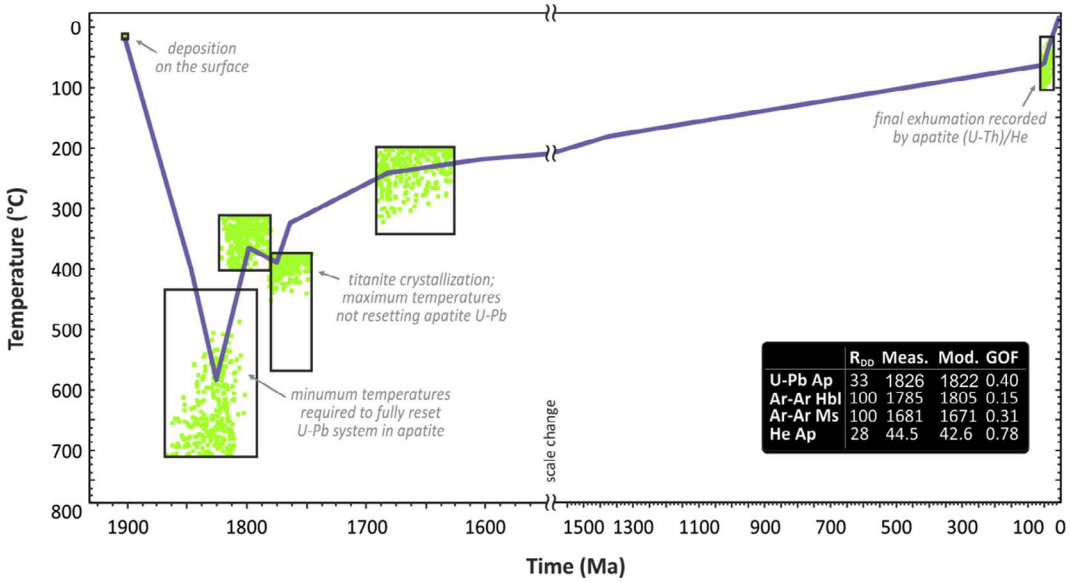

Fig. 6. Thermal history modelling results of available U-Pb, Ar-Ar and (U-Th)/He data displayed in a time-temperature diagram modelled with the HeFTy program (Ketcham, 2005), where the statistically best fitting trajectory is shown as a thick violet line; green dots indicate the values of peak temperatures and inflexion point of thermal trajectories, and black rectangles represent constraints defined according to available geological record (see the text for details). The model was parametrized by the measured apatite U-Pb, hornblende and muscovite Ar-Ar, and apatite (U-Th)/He ages, size of spherical diffusion domains based on measured and assumed physical dimensions of dated crystals, and diffusion kinetic parameters of Cherniak et al. (1991) for apatite U-Pb, Harrison et al. (1991) for hornblende Ar-Ar, Hames and Bowring (1994) for muscovite Ar-Ar, and Farley (2000) for the apatite (U-Th)/He system. Table insets: R_{DD} - radius of the spherical diffusional domain (in μm); Meas. - measured age in Ma; Mod. - modelled age in Ma; GOF - goodness of fit where an acceptable fit corresponds to value 0.5 or higher. (For interpretation of the references to colour in this figure legend, the reader is referred to the web version of this article.)

which apatite grew because:

(a) The higher closure temperature of titanite (c. 700 °C) compared with apatite (c. 450–550 °C) and large grain sizes of titanite would favour preservation of titanite ages, which would be the same or older than apatite formed during the same thermal event, and
(b) Thermal modelling cannot accommodate a simple cooling history.

The interpretation of a punctuated late-orogenic thermal history is strengthened by the recognition of a similar sequence of events in the thermal histories of both the Nagssugtoquidian to the south and in the Quebec-Torngat segment of the Trans-Hudson Orogen to the west. Based on the lithological and isotopic character, age, and inferred geological setting, the Karrat Group has been correlated with the typically higher metamorphic grade Piling and Penrhyn Groups on Baffin Island and the Melville Peninsula (Taylor, 1982; Henderson, 1983). These rocks were intruded by petrogenetically related large felsic plutons at 1900–1870 Ma – the Prøven Igneous Complex and Qikiqtarjuaq suite respectively (Thrane et al., 2005; Thrane, pers comm., 2017). In Greenland, this felsic magmatism was followed by Nagssugtoqidian orogenesis, which records the collision of the North Atlantic and Rae Cratons, beginning with WNW-directed thrusting after 1873 Ma and culminating in crustal thickening and peak metamorphism at c. 1850 Ma (van Gool et al., 1999; Connelly and Mengel, 2000; Connelly et al., 2000).

A 1840–1830 Ma event in the Karrat Group (Thrane et al., 2005: Thrane pers. comm., 2017) is consistent with the emplacement of large bodies of granitic pegmatite and leucogranite at 1838–1835 Ma, synchronous with < 1849 to > 1835 Ma early granulite-facies metamorphism of the Piling Group on Baffin Island (Wodicka et al., 2003; St-Onge et al., 2005, 2007) and widespread growth of metamorphic monazite at ≤1845 Ma (Gagne et al., 2009). Similarly, elevated temperatures throughout the Nagssugtoqidian Orogen are recorded around this time by granitic and pegmatitic magmatism during regional folding at 1825 Ma (Connelly et al., 2000). Connelly et al. (2000) also note that temperatures remained high enough in the Nagssugtoqidian Orogen to produce pegmatites, metamorphic zircon and titanite in the period 1821–1778 Ma, post-dating tectonic fabric development.

Metamorphic resetting of primary magmatic apatite at 1826 ± 9 Ma in the Karrat Group is coincident with 1820–1800 Ma Sm-Nd and Lu-Hf metamorphic garnet ages from the Prøven Igneous Complex (Thrane et al., 2005) and similar in age to a higher temperature thermal and deformation event on Baffin Island attributed to collision of the Rae Craton with the Superior Craton during the Trans-Hudson Orogeny (St-Onge et al., 2007). Peak metamorphism associated with granite plutonism in the Piling Group on Baffin Island occurred at 1812–1810 Ma (Henderson and Henderson, 1994), consistent with the timing of formation of penetrative foliation (≥1806–1800 Ma, unpublished data of R.R Parish in Gagne et al. (2009)). Similarly, several authors have noted a regionally significant episode of monazite growth throughout Baffin Island and the Rae Craton further north at c. 1805 Ma (St-Onge et al., 2005; Gagne et al., 2009).

Metamorphic titanite growth at c. 1768 Ma in the Kangigdleq Member of the Karrat Group was coeval with monazite growth associated with formation of a crenulation cleavage in the Longstaff Bluff Formation of the Piling Group on Baffin Island (Gagne et al., 2009). This metamorphic mineral growth event occurred only shortly after formation of ENE-striking sinistral steep belts in the Nagssugtoqidian during crustal shortening at 1779–1774 Ma, based on zircon lower intercept ages of deformed Archean granites (Connelly et al., 2000). Connelly et al. (2000) also report undeformed pegmatites from the southern and central Nagssugtoqidian Orogen with monazite U-Pb upper intercept ages of 1793 ± 2 Ma, 1784 +10/−3 Ma, and 1790 +3/−2 Ma, which implies that temperatures were high enough at this time to generate pegmatites. Connelly et al. (2000) report titanite U-Pb ages for a range of rock types across the Nagssugtoqidian Orogen that indicate high temperatures in the period 1796–1775 Ma. Additionally, Paleoproterozoic temperatures were insufficient to reset Archean titanite in the northern Nagssuatoqidian Orogen (Connelly et al., 2000). These observations from the Nagssugtoqidian Orogen are consistent with our interpretation that the Karrat Group in the area of this study, c. 300 km further north, did not reach temperatures above the Pb closure temperature for titanite, or temperatures at which the apatite U-Pb system could be reset again (c. 550 °C).

Our study suggests that the same polymetamorphic history that affected the Quebec-Baffin segment of the Trans-Hudson Orogen on Baffin Island, and which is reflected in the late orogenic history of the Nagssugtoqidian Orogen, also affected the Karrat Group in the Rinkian Orogen, but at a lower metamorphic grade. These data indicate that there is a shared tectonic history extending over 100 million years related to Paleoproterozoic orogenesis over a regional extent of more than 500 × 1000 km.

6.4. Implications for geochronology common Pb bearing phases

The common Pb component within titanite from the Karrat mafic metavolcanics is significantly different in composition to that trapped within apatite in the same rock. Apatite common Pb has a $^{207}Pb/^{206}Pb$ ratio similar to 1826 Ma Stacey and Kramers (1975) model common Pb, implying the incorporation of Pb into the crystal structure from the magmatic environment during apatite crystallization. More specifically the $^{207}Pb/^{204}Pb$ versus $^{206}Pb/^{204}Pb$ plane derived through a 3D planar fit to the data from apatite sample 571721, suggests that a source with higher Mu ($^{238}U/^{204}Pb$) than Stacey and Kramers terrestrial Pb model was present in the magmatic environment in which this apatite grew (Fig. 7). This implies an ancient radiogenic upper crustal source of common Pb in the immediate environment of the Karrat mafic volcanics, consistent with the presence of Archean supercrustal material in the region and as detritus within both the Qeqertarssuaq and Nûkavsak Formations (Kalsbeek et al., 1998; Thrane pers. comm. 2017), and suggests interaction of this material with the Karrat volcanic system.

During diffusive re-equilibration of apatite at c. 1826 Ma, it is feasible that common Pb was incorporated into the grain. The composition of this common Pb would reflect the components that were diffusively mobile within the rock during this thermal episode. However, such a process would require Pb gain in apatite and would destroy any

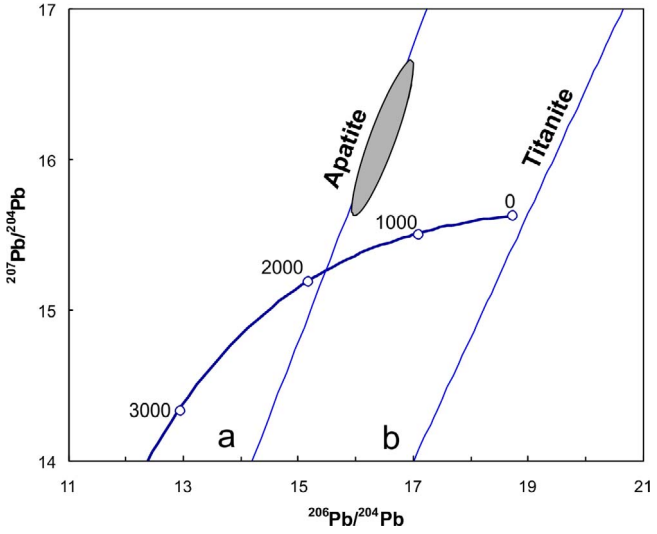

Fig. 7. Plot of $^{207}Pb/^{204}Pb$ versus $^{206}Pb/^{204}Pb$ showing the location of the best estimate of common Pb from the 3D regression of apatite data for sample 571721. The average for all apatite samples common $^{207}Pb/^{206}Pb$ determined from upper intercepts in the Tera and Wasserburg concordia diagram is shown as isochron (a) whereas for titanite it is shown as isochron (b). Data point error ellipse is at the two sigma level. The Stacey and Kramers (1975) terrestrial Pb growth curve is shown.

common-radiogenic mixing lines with chronometric significance. Given the well-defined mixing lines in U-Pb space, we interpret U-Pb resetting of apatite as being due to radiogenic- Pb loss with no in-diffusion. It follows that the composition of the trapped common Pb should have a signature indicative of the original crystallization environment. Although there is the potential for significant complexity in diffusional processes, likely governed to some extent by surrounding minerals, we suggest the fact that the common $^{207}Pb/^{206}Pb$ value in the apatite closely matches that of 1800–1900 model Pb is consistent with a Pb loss process rather than gain of an extraneous common Pb component during diffusive resetting.

In contrast to apatite common $^{207}Pb/^{206}Pb$ values, titanite shows dramatically lower ratios, slightly lower than even modern common Pb compositions (Stacey and Kramers, 1975; Fig. 7). During analysis there was no indication of downhole change in ^{204}Pb counts, which could be indicative of surface derived contamination. Rather, it is feasible that the metamorphic titanite formed from breakdown of pre-existing Ti-rich minerals such as rutile or ilmenite. Any precursor phase containing U (e.g. rutile, perovskite) would have generated radiogenic-Pb over the time interval between igneous crystallization and metamorphic recrystallization and such Pb would have a much lower $^{207}Pb/^{206}Pb$ ratio than common Pb. The presence of some of this ancient Pb in the metamorphic titanite would lower the $^{207}Pb/^{206}Pb$ ratio of the initial Pb, giving it a composition more similar to recent Pb in common Pb evolution models. There is no reason to expect that remobilized Pb in a metamorphic environment would have an isotopic composition reflective of the whole rock nor a crustal Pb model, rather it would be reflective of the proportion, age and Mu values of whatever minerals were breaking down at the time of metamorphism. Nonetheless, we contend that it is feasible to use common Pb as a tracer to help understand the growth or alternation mechanism when there is highly distinct compositions as in our case study with clear difference between the metamorphic and igneous common Pb reservoirs.

7. Conclusions

Four samples were collected from metavolcanic rocks, interpreted as mafic lavas and tuffs, of the Kangigdleq Member of the Nûkavsak Formation, Greenland. Excluding one sample, in which no titanite was recovered, both titanite and apatite grains were analysed by LA-ICPMS in order to constrain the thermal history for the Rinkian Orogen.

Apatite in these samples occurs as equant, euhedral to subhedral crystals partially enclosed in the major primary minerals, consistent with a primary magmatic origin. U-Pb data from these apatite samples indicate they are mixtures between radiogenic and common Pb. The best estimate of the age of the radiogenic-Pb component in all apatite samples is similar, with a weighted mean age of 1826 ± 9 Ma. Given the relatively low closure temperature of the apatite system, the known metamorphic history of the region and the consistent apatite U-Pb ages, the apatite dates are interpreted to reflect resetting of the U-Pb system after magmatic crystallization, rather than some partial Pb loss process.

Titanite from the metavolcanic rocks is anhedral, irregular, elongated parallel to the metamorphic foliation, and holds inclusions of apatite. In contrast, apatite does not contain inclusions of titanite. The REE pattern for titanite is characterized by low total REE content, positive Eu anomalies, and depletion in both heavy and light REE, consistent with a metamorphic-hydrothermal genesis. All titanite samples indicate mixtures between common and radiogenic-Pb components. Best estimates for the radiogenic component are similar for all samples with a weighted mean age of 1768 ± 8 Ma. As the titanite U-Pb date is younger than the apatite U-Pb date we interpret the titanite age to reflect metamorphic crystallization rather than cooling.

Apatite from one of the samples yielded a (U-Th)/He age of 46 ± 7 Ma, interpreted as the time of cooling through ~80–40 °C. Using this new geochronology, published constraints from other isotopic systems, and knowledge of isotope diffusion parameters for the measured grain size, we modelled the thermal evolution for this part of the Rinkian Orogen. Thermal modelling indicates that the minimum temperatures reached during a first thermal event at ≥1826 Ma must have exceeded 485 °C. Furthermore, a second heating event that did not exceed 452 °C is recorded by crystallization of titanite at c. 1768 Ma.

The resetting of magmatic apatite is interpreted to be a response to collision between the Rae Craton and the Superior Craton during the Trans-Hudson Orogeny. Subsequent metamorphic titanite growth at c. 1768 Ma is interpreted as distal evidence of an event similar to those late in the orogenic history of the Nagssugtoqidian Orogen, albeit at a lower metamorphic grade. These results show a shared tectonic history extending over 100 million years between the Nagssugtoqidian and Rinkian Orogens related to Paleoproterozoic events over a regional extent of more than 500 x 1000 km.

Accurate age determination is dependent on accounting for the common Pb content in both apatite and titanite. Intriguing results from this work suggest significantly different common Pb compositions for these phases. Specifically, all apatite samples yield similar upper intercepts with $^{207}Pb/^{206}Pb$ ratios comparable to 1800 Ma common Pb of the Stacey and Kramers (1975) Pb model, consistent with ancient common Pb incorporation during magmatic crystal growth. In stark contrast, all titanite samples yield upper intercepts that have distinctly lower $^{207}Pb/^{206}Pb$ ratios, even less than typical modern day common Pb. The common Pb cargo of this metamorphic titanite appears to reflect a mixture of precursor radiogenic-Pb from recrystallized minerals and ancient common Pb. The distinctly different common Pb composition of the titanite crystals provides an indication that the growth environment of this mineral was dissimilar to magmatic apatite. Additionally the common Pb signature indicates a titanite growth mechanism involving redistribution of radiogenic-Pb during metamorphic recrystallization of precursor U bearing minerals.

Acknowledgements

The authors thank F. Corfu, K. Thrane, D. Rosa and A. Kylander-Clark for constructive comments. D. Davis is especially thanked for numerous pertinent comments that have significantly enhanced this work. Lærke Louise Thomsen is thanked for contribution to the field work. The authors also thank TSW Analytical, Perth for access to the Agilent 7500 for U and Th analysis during (U-Th)/He dating. This study forms part of a project co-financed by the Government of Greenland and the Geological Survey and Denmark and Greenland.

Appendix A. Supplementary data

Supplementary data associated with this article can be found, in the online version, at http://dx.doi.org/10.1016/j.precamres.2017.07.033.

References

Aleinikoff, J.N., Wintsch, R., Tollo, R.P., Unruh, D.M., Fanning, C.M., Schmitz, M.D., 2007. Ages and origins of rocks of the Killingworth dome, south-central Connecticut: implications for the tectonic evolution of southern New England. Am. J. Sci. 307 (1), 63–118.

Allen, C.R., Harris, C.J., 1980. Year-end report 1979, Karrat Group reconnaissance program, Marmorilik area, west Greenland. GEUS report. file number 20435.

Andersen, T., 2002. Correction of common lead in U-Pb analyses that do not report 204Pb. Chem. Geol. 192 (1–2), 59–79.

Broska, I., Harlov, D., Tropper, P., Siman, P., 2007. Formation of magmatic titanite and titanite–ilmenite phase relations during granite alteration in the Tribeč Mountains, Western Carpathians, Slovakia. Lithos 95 (1–2), 58–71.

Catanzaro, E.J., Hanson, G.N., 1971. U–Pb ages for sphene from early Precambrian igneous rocks in northeastern minnesota–northwestern Ontario. Can. J. Earth Sci. 8 (10), 1319–1324.

Chamberlain, K.R., Bowring, S.A., 2001. Apatite–feldspar U-Pb thermochronometer: a reliable, mid-range (~450°C), diffusion-controlled system. Chem. Geol. 172 (1–2), 173–200.

Che, X.D., Linnen, R.L., Wang, R.C., Groat, L.A., Brand, A.A., 2013. Distribution of trace and rare earth elements in titanite from tungsten and molybdenum deposits in Yukon and British Columbia, Canada. Can. Mineral. 51 (3), 415–438.

Cherniak, D.J., 1993. Lead diffusion in titanite and preliminary results on the effects of radiation damage on Pb transport. Chem. Geol. 110 (1–3), 177–194.
Cherniak, D.J., Watson, E.B., 2000. Pb diffusion in rutile. Contrib. Miner. Petrol. 139 (2), 198–207.
Cherniak, D.J., Watson, E.B., 2001. Pb diffusion in zircon. Chem. Geol. 172 (1–2), 5–24.
Cherniak, D.J., Lanford, W.A., Ryerson, F.J., 1991. Lead diffusion in apatite and zircon using ion implantation and Rutherford Backscattering techniques. Geochim. Cosmochim. Acta 55 (6), 1663–1673.
Chew, D.M., Sylvester, P.J., Tubrett, M.N., 2011. U–Pb and Th–Pb dating of apatite by LA-ICPMS. Chem. Geol. 280 (1–2), 200–216.
Chew, D.M., Petrus, J.A., Kamber, B.S., 2014. U–Pb LA–ICPMS dating using accessory mineral standards with variable common Pb. Chem. Geol. 363, 185–199.
Compston, W., Williams, I.S., Kirschvink, J.L., Zichao, Z., Guogan, M.A., 1992. Zircon U-Pb ages for the Early Cambrian time-scale. J. Geol. Soc. 149 (2), 171–184.
Connelly, J.N., Mengel, F.C., 2000. Evolution of Archean components in the Paleoproterozoic Nagssugtoqidian orogen, West Greenland. Geol. Soc. Am. Bull. 112 (5), 747–763.
Connelly, J.N., Thrane, K., 2005. Rapid determination of Pb isotopes to define Precambrian allochthonous domains: an example from West Greenland. Geology 33 (12), 953–956.
Connelly, J.N., van Gool, J.A.M., Mengel, F.C., 2000. Temporal evolution of a deeply eroded orogen: the Nagssugtoqidian Orogen, West Greenland. Can. J. Earth Sci. 37 (8), 1121–1142.
Connelly, J.N., Thrane, K., Krawiec, A.W., Garde, A.A., 2006. Linking the Palaeoproterozoic Nagssugtoqidian and Rinkian orogens through the Disko Bugt region of West Greenland. J. Geol. Soc. 163 (2), 319–335.
Corfu, F., 1988. Differential response of U-Pb systems in coexisting accessory minerals, Winnepeg River Subprovince, Canadian Shield: Implications for Archean crustal growth and stabilization. Contrib. Miner. Petrol. 98 (3), 312–325.
Corfu, F., 1996. Multistage zircon and titanite growth and inheritance in an Archean gneiss complex, Winnipeg River Subprovince, Ontario. Earth Planet. Sci. Lett. 141 (1–4), 175–186.
Cumming, G.L., Richards, J.R., 1975. Ore lead isotope ratios in a continuously changing earth. Earth Planet. Sci. Lett. 28 (2), 155–171.
Danišík, M., Kuhlemann, J., Dunkl, I., Evans, N.J., Székely, B., Frisch, W., 2012a. Survival of ancient landforms in a collisional setting as revealed by combined fission track and (U-Th)/He thermochronometry: a case study from Corsica (France). J. Geol. 120 (2), 155–173.
Danišík, M., Štěpančíková, P., Evans, N.J., 2012b. "Constraining long-term denudation and faulting history in intraplate regions by multisystem thermochronology: An example of the Sudetic Marginal Fault (Bohemian Massif, central Europe)". Tectonics 31 (2). http://dx.doi.org/10.1029/2011TC003012. TC2003.
Dodson, M.H., 1973. Closure temperature in cooling geochronological and petrological systems. Contrib. Miner. Petrol. 40 (3), 259–274.
Dodson, M.H., 1986. Closure profiles in cooling systems. Mater. Sci. Forum 7, 145–154.
Escher, J.C. (compiler), 1980, Map sheet no. 4, Upernavik Isfjord, 1: 500.000, Geological Map of Greenland, Geological Survey of Greenland.
Escher, J.C., 1985. "Map sheet no. 4, Upernavik Isfjord Compilation". Geological Maps of Greenland on CD-ROM. Geological Survey of Denmark and Greenland.
Essex, R.M., Gromet, L.P., 2000. U-Pb dating of prograde and retrograde titanite growth during the Scandian orogeny. Geology 28 (5), 419–422.
Farley, K.A., 2000. Helium diffusion from apatite: general behavior as illustrated by Durango fluorapatite. J. Geophys. Res. Solid Earth 105 (B2 no. B2), 2903–2914.
Gagne, S., Jamieson, R.A., MacKay, R., Wodicka, N., Corrigan, D., 2009. Texture, composition, cand age variations in monazite from the lower amphibolite to the granulite facies, Longstaff Bluff Formation, Baffin Island, Canada. Can. Mineral. 47 (4), 847–869.
Gallagher, K., 2012. Transdimensional inverse thermal history modeling for quantitative thermochronology. J. Geophys. Res. Solid Earth 117 (B2).
Garde, A.A., Pulvertaft, T.C.R., 1976. Age relations of the Precambrian Mârmorilik Marble Formation, central West Greenland. Rapp. Grønl. Geol. Unders. 80, 49–53.
Garde, A.A., Grocott, J., Thrane, K., Connelly, J.N., 2003, Reappraisal of the Rinkian fold belt in central West Greenland: Tectonic evolution during crustal shortening and linkage with the Nagssugtoqidian orogen. Geophysical research Abstracts 5 (EGS-AGU-EUG Joint Assembly), 09411.
Gibson, G.M., Ireland, T.R., 1996. Extension of Delamerian (Ross) orogen into western New Zealand: Evidence from zircon ages and implications for crustal growth along the Pacific margin of Gondwana. Geology 24 (12), 1087–1090.
Grocott, J., Pulvertaft, T.C.R., 1990. "The Early Proterozoic Rinkian Belt of Central West Greenland". In The Early Proterozoic Trans-Hudson Orogen of North America. vol. 37. ed. J. F. Lewry and M. R. Stauffer, 443–463. Geological Association of Canada Special Paper.
Gromet, L.P., 1991, "Direct dating of deformational fabrics". L. Heaman, J.N. Ludden (Eds), Applications of Radiogenic Isotope Systems to Problems in Geology, Mineral. Assoc. Can., Short Course Handbook, 19 (1991), pp. 167–189.
Hames, W.E., Bowring, S.A., 1994. An empirical evaluation of the argon diffusion geometry in muscovite. Earth Planet. Sci. Lett. 124 (1–4), 161–167.
Hanson, G.N., Catanzaro, E.J., Anderson, D.H., 1971. U–Pb for sphene in a contact metamorphic zone. Earth Planet. Sci. Lett. 12 (2), 231–237.
Harrison, T.M., Lovera, O.M., Heizler, M.T., 1991. 40Ar/39Ar results for alkali felspars containing diffusion domains with differing activation energy. Geochim. Cosmochim. Acta 55 (5), 1435–1448.
Henderson, J.R., 1983. Structure and metamorphism of the Aphebian Penrhyn Group and its Archean basement complex in the Lyon Inlet area, Melville Peninsula, District of Franklin. vol. 324. Geological Survey of Canada Bulletin. doi: http://dx.doi.org/10.4095/119500.
Henderson, J.R., Henderson, M.N., 1994. Geology of the Dewar Lakes area, central Baffin Island, District of Franklin, N.W.T. (parts of 27B and 37A). Geological Survey of Canada Open File 2924 (scale 1:100,000).
Henderson, G., Pulvertaft, T.C.R., 1967. The stratigraphy and structure of the Precambrian rocks of the Umanak area, West Greenland. Meddelelser fra Dansk Geologisk Forening 17, 1–22.
Henderson, G., Pulvertaft, T.C.R., 1987. Geological map of Greenland, 1:100 000, Mârmorilik 71 V. 2 Syd, Nûgâtsiaq 71 V.2 Nord and Pangnertôq 72 V.2 Syd, descriptive text. Geological Survey of Greenland, Copenhagen, 72 pp.
Housh, T., Bowring, S.A., 1991. Lead isotopic heterogeneities within alkali feldspars: Implications for the determination of initial lead isotopic compositions. Geochim. Cosmochim. Acta 55 (8), 2309–2316.
Johns, S.M., 2002. Nd Isotope Constraints on the Provenance and Tectonic Evolution of the Piling Group Metasedimentary Rocks, Baffin Island, Nunavut. B.Sc. thesis, University of Saskatchewan, Saskatoon, Saskatchewan.
Kalsbeek, F., Pulvertaft, T.C.R., Nutman, A.P., 1998. Geochemistry, age and origin of metagreywackes from the Palaeoproterozoic Karrat Group, Rinkian Belt, West Greenland. Precambr. Res. 91 (3–4), 383–399.
Kennedy, Allen K., Kamo, Sandra L., Nasdala, Lutz., Timms, Nicolas E., 2010. Grenville Skarn Titanite: Potential Reference Material for Sims U-Th–Pb Analysis. Can. Mineral. 48 (6), 1423–1443.
Ketcham, R.A., 2005. Forward and inverse modeling of low-temperature thermochronometry data. Rev. Mineral. Geochem. 58 (1), 275–314.
Kirkland, C.L., Spaggiari, C.V., Johnson, T.E., Smithies, R.H., Danišík, M., Evans, N., Wingate, M.T.D., et al., 2016. Grain size matters: implications for element and isotopic mobility in titanite. Precambr. Res. 278, 283–302.
Kohn, M.J., Corrie, S.L., 2011. Preserved Zr-temperatures and U-Pb ages in high-grade metamorphic titanite: Evidence for a static hot channel in the Himalayan orogen. Earth Planet. Sci. Lett. 311 (1–2), 136–143.
Krogstad, E.J., Walker, R.J., 1994. High closure temperatures of the U-Pb system in large apatites from the Tin Mountain pegmatite, Black Hills, South Dakota. Geochim. Cosmochim. Acta 58 (18), 3845–3853.
Larsen, L.M., Pedersen, A.K., Tegner, C., et al., 2016. Age of Tertiary volcanic rocks on the West Greenland continental margin: volcanic evolution and event correlation to other parts of the North Atlantic Igneous Province. Geol. Mag. 153, 487–511.
Ludwig, K.R., 1998. On the treatment of concordant uranium–lead ages. Geochim. Cosmochim. Acta 62 (4), 665–676.
Mezger, K., Hanson, G.N., Bohlen, S.R., 1989. High-precision U-Pb ages of metamorphic rutile: Application to the cooling history of high-grade terranes. Earth Planet. Sci. Lett. 96 (1–2), 106–118.
Mezger, K., Essene, E.J., van der Pluijm, B.A., Halliday, A.N., 1993. U-Pb geochronology of the Grenville Orogen of Ontario and New York: Constraints on ancient crustal tectonics. Contrib. Miner. Petrol. 114 (1), 13–26.
Morad, S., El-Ghali, M.A.K., Caja, M.A., Al-Ramadan, K., Mansurbeg, H., 2009. Hydrothermal alteration of magmatic titanite: evidence from proterozoic granitic rocks, southeastern Sweden. Can. Mineral. 47 (4), 801–811.
Mott, A.V., Bird, D.K., Grove, M., Rose, N., Bernstein, S., Mackay, H., Krebs, J., 2013. Karrat Isfjord: A Newly Discovered Paleoproterozoic Carbonatite-Sourced REE Deposit, Central West Greenland. Econ. Geol. Bull. Soc. Econ. Geol. 108 (6), 1471–1488.
Oosthuyzen, E.J., Burger, A.J., 1973. The suitability of apatite as an age indicator by the uranium–lead isotope method. Earth Planet. Sci. Lett. 18 (1), 29–36.
Paton, C., Woodhead, J.D., Hellstrom, J.C., Hergt, J.M., Greig, A., Maas, R., 2010, Improved laser ablation U-Pb zircon geochronology through robust downhole fractionation correction: Geochemistry Geophysics Geosystems (G3), 11, paper number Q0AA06, doi: 10.1029/2009GC002618.
Pidgeon, R.T., Bosch, D., Bruguier, O., 1996. Inherited zircon and titanite U-Pb systems in an Archaean syenite from southwestern Australia: Implications for U-Pb stability of titanite. Earth Planet. Sci. Lett. 141 (1–4), 187–198.
Rasmussen, H., Holm, P.M., 1999. "Proterozoic thermal activity in the Archean basement of the Disko Bugt region and eastern Nuussuaq, West Greenland": evidence from K-Ar and 40Ar-39Ar mineral age investigations' Geology of Greenland. Survey Bulletin 181, 55–64.
Rosa, D., Guarnieri, P., Hollis, J., Kolb, J., Partin, C., Petersen, J., Sørensen, E.V., Thomassen, B., Thomsen, L.L., Thrane, K., 2016. "Architecture and mineral potential of the Paleoproterozoic Karrat Group, West Greenland: Results of the 2015 season". Danmarks og Grønlands Geologiske Undersøgelse Rapport 2016/12.
Schmitz, M.D., Bowring, S.A., Ireland, T.R., 2003. Evaluation of Duluth Complex anorthositic series (AS3) zircon as a U-Pb geochronological standard: New high-precision isotope dilution thermal ionization mass spectrometry results. Geochim. Cosmochim. Acta 67 (19), 3665–3672.
Schoene, B., Bowring, S.A., 2006. U–Pb systematics of the McClure Mountain syenite: Thermochronological constraints on the age of the 40Ar/39Ar standard MMhb. Contrib. Miner. Petrol. 151 (5), 615–630.
Schwartz, J.J., Stowell, H.H., Klepeis, K.A., Tulloch, A.J., Kylander-Clark, A.R.C., Hacker, B.R., Coble, M.A., 2016. Thermochronology of extensional orogenic collapse in the deep crust of Zealandia. Geosphere 12 (3), 647–677.
Scott, D.J., St-Onge, M.R., 1995. Constraints on Pb closure temperature in titanite based on rocks from the Ungava Orogen, Canada; implications for U-Pb geochronology and P-T-t path determinations. Geology 23 (12), 1123–1126.
Sidgren, A.S., Page, L., Garde, A.A., 2006. New hornblende and muscovite 40Ar/39Ar cooling ages in the central Rinkian fold belt, West Greenland. Geol. Surv. Denmark Greenland Bulletin 11, 115–123.
Spencer, K.J., Hacker, B.R., Kylander-Clark, A.R.C., Andersen, T.B., Cottle, J.M., Stearns, M.A., Poletti, J.E., Seward, G.G.E., 2013. Campaign-style titanite U-Pb dating by laser-ablation ICP: Implications for crustal flow, phase transformations and titanite

closure. Chem. Geol. 341, 84–101.
Stacey, J.C., Kramers, J.D., 1975. Approximation of terrestrial lead isotope evolution by a two-stage model. Earth Planet. Sci. Lett. 26 (2), 207–221.
St-Onge, M.R., Scott D.J., Corrigan D., Wodicka, N., 2005. "Geology, central Baffin Island, Nunavut. Geological Survey of Canada Maps 2077A to 2082A" (scale 1:100,000).
St-Onge, M.R., Wodicka, N., Ijewliw, O., 2007. Polymetamorphic evolution of the Trans-Hudson Orogen, Baffin Island, Canada: Integration of petrological, structural and geochronological data. J. Petrol. 48 (2), 271–302.
St-Onge, M.R., van Gool, J.A.M., Garde, A.A., Scott, D.J., 2009. "Correlation of Archaean and Palaeoproterozoic units between northeastern Canada and western Greenland: constraining the pre-collisional upper plate accretionary history of the Trans-Hudson orogeny". In: Cawood P.A. and Kroner A. (Eds) Earth Accretionary Systems in Space and Time. The Geological Society, London, Special Publications, 318, pp. 193–235, DOI: 10.1144/SP318.7.
Storey, C.D., Jeffries, T.E., Smith, M., 2006. Common lead-corrected laser ablation ICP-MS U-Pb systematics and geochronology of titanite. Chem. Geol. 227 (1–2), 37–52.
Taylor, B.E., 1982. "Precambrian geology of the Canadian north borderlands". In: Geology of the North Atlantic Borderlands (J.W. Kerr, A.J. Fergusson & L.C. Machan, eds.). Can. Soc. Petrol. Geol., Memoir 7: 11–30.
Tera, F., Wasserburg, G.J., 1972. U–Th–Pb systematics in lunar highland samples from the Luna 20 and Apollo 16 missions. Earth Planet. Sci. Lett. 17 (1), 36–51.
Thomson S.N., Gehrels, G.E., Ruiz, J., Buchwaldt, R., 2012. "Routine low-damage U-Pb dating of apatite using laser ablation-multicollector-ICPMS". Geochemistry, Geophysics, Geosystems, 13, Q0AA21, doi: http://dx.doi.org/10.1029/2011GC003928.
Thrane, K., Connelly, J.N., Garde, A.A., Grocott, J., Krawiec, A.W., 2003. Linking the Palaeoproterozoic Rinkian and Nagssugtoqidian belts of central West Greenland: Implications of new U-Pb and Pb-Pb zircon ages. Geophys. Res. Abstr. 5, 09275.
Thrane, K., Baker, J., Connelly, J., Nutman, A., 2005. Age, petrogenesis and metamorphism of the syn-collisional Prøven Igneous Complex, West Greenland. Contrib. Miner. Petrol. 149 (5), 541–555.
Tilton, G.R., Grunenfelder, M.H., 1968. Sphene: Uranium–lead ages. Science 159 (3822), 1458–1461.
Tucker, R.D., Raheim, A., Krogh, T.E., Corfu, F., 1986. Uranium–lead zircon and titanite ages from the northern portion of the Western Gneiss Region, south-central Norway. Earth Planet. Sci. Lett. 81 (2–3), 203–211.
van Gool, J.A.M., Kriegsman, L., Marker, M., Nichols, G.T., 1999. Thrust stacking in the inner Nordre Strømfjord area, West Greenland: significance for the tectonic evolution of the Paleoproterozoic Nagssugtoqidian orogen. Precambr. Res. 93 (1), 71–86.
van Gool, J.A.M., Connelly, J.N., Marker, M., Mengel, F.C., 2002. The Nagssugtoqidian Orogen of West Greenland: Tectonic evolution and regional correlations from a West Greenland perspective. Can. J. Earth Sci. 39 (5), 665–686.
Webster, J.D., Piccoli, P.M., 2015. Magmatic apatite: a powerful, yet deceptive, mineral. Elements 11 (3), 177–182.
Williams, I.S., 1998. "U–Th–Pb geochronology by ion microprobe". In: Applications of Microanalytical Techniques to Understanding Mineralizing Porcesses. vol. 7. ed. M. A. McKibben, W. C. Shanks, III, and W. I. Ridley, 1–35. Reviews in Economic Geology. Littleton, CO: Society of Economic Geologists.
Willigers, B.J.A., Baker, J.A., Krogstad, E.J., Peate, D.W., 2002. Precise and accurate in situ Pb–Pb dating of apatite, monazite, and sphene by laser ablation multiple-collector ICP-MS. Geochim. Cosmochim. Acta 66 (6), 1051–1066.
Wodicka, N., St-Onge, M.R., Corrigan, D., Scott, D.J., 2003. "Tectonothermal evolution of Archean basement and Paleoproterozoic cover in central Baffin Island, Nunavut: Constraints from U-Pb geochronology. Geol. Assoc. Can. – Mineral. Assoc. Can". Program with Abstracts (Geological Association of Canada) 28:648.
Xie, L., Wang, R.C., Chen, J., Zhu, J.C., 2010. Mineralogical evidence for magmatic and hydrothermal processes in the Qitianling oxidized tin-bearing granite (Hunan, South China): EMP and (MC)-LA-ICPMS investigations of three types of titanite. Chem. Geol. 276 (1–2), 53–68.